CHALMERS
UNIVERSITY OF TECHNOLOGY

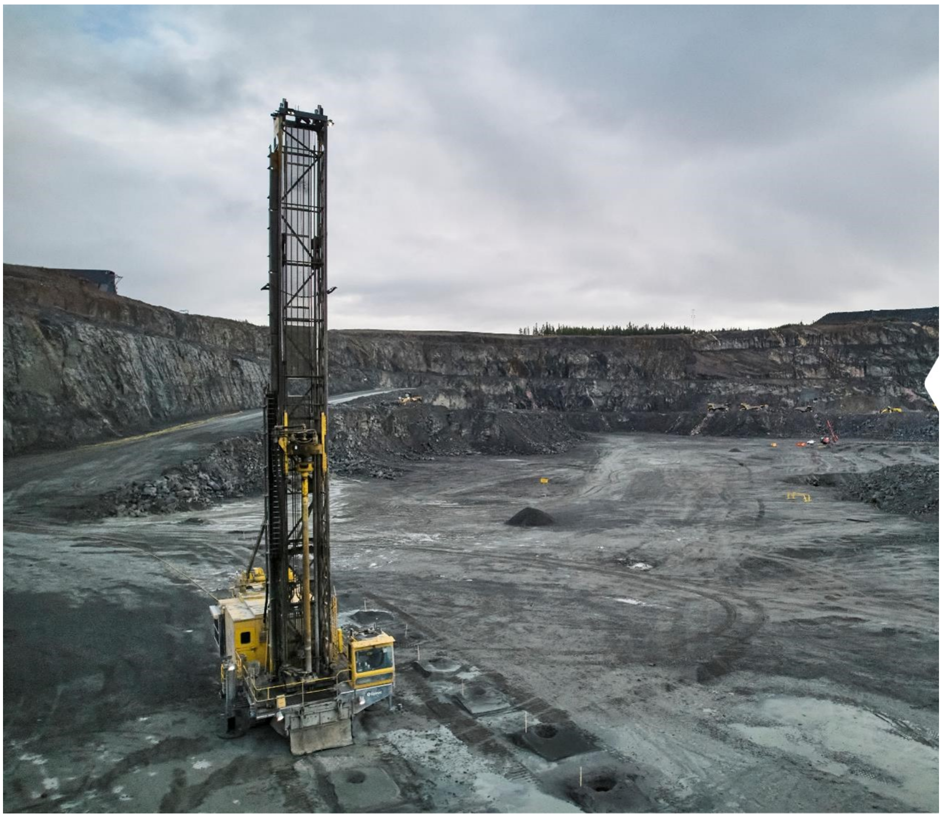

Voltage support in open pit mining power systems using electric drill rigs

Master's thesis in Sustainable Electric Power Engineering and Electromobility

JAIME ANDRES PARDO GALVIS
JUAN PABLO GOMEZ ARGÜELLO

DEPARTMENT OF ELECTRICAL ENGINEERING
CHALMERS UNIVERSITY OF TECHNOLOGY
Gothenburg, Sweden 2025
www.chalmers.se

Master's thesis 2025

Master's thesis in Sustainable Electric Power Engineering and Electromobility

JAIME ANDRES PARDO GALVIS
JUAN PABLO GOMEZ ARGÜELLO

Department of Electrical Engineering
Division of Electric Power Engineering
Chalmers University of Technology
Gothenburg, Sweden 2025

Master's thesis in Sustainable Electric Power Engineering and Electromobility
JAIME ANDRES PARDO GALVIS
JUAN PABLO GOMEZ ARGÜELLO

Supervisor: Ritwik Majunder, Sr. Principal Engineer at Epiroc
Examiner: Peiyuan Chen, Department of Electrical Engineering

Master's Thesis 2025
Department of Electrical Engineering
Division of Electric Power Engineering
Chalmers University of Technology
SE-412 96 Gothenburg
Telephone +46 31 772 1000

Cover: EPIROC's viper drilling platform.

Typeset in LaTeX
Gothenburg, Sweden 2025

Abstract

The electrification of mining operations presents significant challenges in power quality, particularly in remote open-pit mines where limited grid connectivity results in reduced short-circuit capacity and increased susceptibility to voltage instability. High-power induction motor startups in drilling equipment frequently generate significant voltage sags, that compromise operational continuity and compliance with power quality standards.

This thesis examines different configurations of the motor and drive system for electric drilling units and their impact on voltage profiles in mining grids. The study aims to determine how electric drillers can provide voltage support to improve grid voltage stability. A comprehensive electrical distribution grid model was developed in MATLAB/Simulink, incorporating typical mining environment loads. Critical scenarios were identified through parametric sweeps across different grid strengths to assess voltage sag depth, duration, and reactive power demand under multiple operational scenarios.

Simulation results demonstrate that Active Front End (AFE) drives significantly reduce the severity of voltage sag, improve steady-state voltage profiles, and maintain system stability under weak grid conditions. When AFE control is modified to provide dynamic reactive power compensation, additional voltage support is achieved, further mitigating voltage sags and enabling stable operation under even weaker grid conditions while maintaining voltage performance comparable to full AFE implementation.

A key contribution of this work is to demonstrate that a single AFE-equipped driller with compensation capability can effectively support multiple Direct-On-Line (DOL) drillers during simultaneous operation, keeping Point-of-Common Coupling (PCC) voltages within acceptable limits without requiring full fleet AFE conversion. This selective deployment approach represents a technically robust and operationally viable solution to enhance power quality and resilience in mining electrical systems.

Keywords: Active Frond End, Voltage Sags, Electric Blast Drillers, Grid Strength, Short Circuit Ratio, Open Pit Mines, Voltage Stability, Reactive Power.

Acknowledgements

We would like to express our gratitude to Epiroc for giving us the opportunity to work and deepened our knowledge in this topic and supporting us in the development of this project. We also extend our heartfelt gratitude to our supervisors at Epiroc Ritwik Majumder, Suresh S and Harshita Konidena for their guidance and support throughout the entire project.

We extend our sincere gratitude to Peiyuan Chen, docent at Chalmers University of Technology for oversee this research. His guidance and encouragement during the project proved to be invaluable.

From Jaime's side.
I am extremely grateful to my wife, Monica. Without her unconditional love, patience, and support, this achievement would not have been possible. Her constant encouragement and belief in me have been an invaluable source of motivation and strength.

I am deeply grateful to my family — Eliberto, Ana, Angelica, Alexis, Sebastian, Omar, and Elsa — for their unwavering support, guidance, and sacrifices, which have enabled me to pursue my goals with confidence and determination.

My heartfelt gratitude goes to my friend Juan Pablo, with whom I had the pleasure of spending my time at Chalmers—filled with laughter, dancing, friendship, and memories that will last forever.

To my friends, thank you for your encouragement, understanding and advice. This thesis would not have been possible without the collective love, understanding, and support of my wife, family, and friends. To all of you, I extend my deepest appreciation.

From Juan Pablo's side.

I am eternally grateful and indebted to my family—Omaira, Ciro, and María Alejandra—my mom, dad, and sister, who have supported me at every stage of my personal and professional life. This milestone is also yours. I hope you feel as proud as I do, because none of this would have been possible without you.

To my Latin friends in Gothenburg—Juan Pablo, Aura, Evelyn, Tania, Monica and Citlali. Inmensamente feliz y agradecido de que la vida nos haya cruzado caminos. Atesoro cada momento que hemos compartido como grupo y de manera individual. En Suecia o en cualquier parte del mundo, siempre podrán contar conmigo, así como yo sé que puedo contar con ustedes. Gracias por ser mi hogar lejos de casa.

To Jaime. Man, gracias de corazón por ser mi compañero y amigo durante estos dos años de aventura. Thanks for the support, the laughs, the stressful moments we got through, and your dedication to this project. I truly hope life lets us cross paths again and work together once more.

Till Sverige och mina svenska vänner. Tack så mycket för att ni har öppnat era dörrar för mig och låtit mig lära känna ert land, er kultur och ert sätt att se världen. Jag är tacksam för allt jag har lärt mig och alla minnen vi har skapat.

This journey has shaped not only my knowledge but also the person I am today. To everyone who walked beside me—tack, gracias, thank you.

Jaime Andres Pardo Galvis
Juan Pablo Gomez Arguello
Gothenburg, August 2025

Contents

List of Acronyms

Below is the list of acronyms that have been used throughout this thesis listed in alphabetical order:

BES	Battery Energy Storage
DER	Distributed Energy Resource
MILP	Mixed-Integer Linear Programming
MG	Microgrid
PV	Photovoltaic
RES	Renewable-based Energy Sources
Freq	Frequency
Prim Wind Res	Primary Winding Resistance
Sec Wind Res	Secondary Winding Resistance
Prim Leak Reac	Primary Leakage Winding Reactance
Sec Leak Reac	Secondary Leakage Winding Reactance
Zero Seq Reac	Zero Sequence Reactance
AFE	Active Front End
DOL	Direct On Line
GSR	Grid Strength Ratio
SCC	Short Circuit Capacity
PCC	Point of common Coupling
STX	Feeder Transformer Rating

List of Figures

List of Tables

1
Introduction

The mining industry has traditionally been a significant contributor to carbon dioxide emissions due to its reliance on diesel-powered machinery (include reference). The principal mining processes such as extraction, material handling, and mineral processing heavily depend on these machines, which generate emissions, heat and diesel fumes that impact negatively on the work environment for mine workers. Furthermore, mining sites are often located in remote areas with limited access to the electrical grid or connected to weak grids, making it necessary to use diesel-powered generators to support operations.

As the world transitions toward fossil-free energy, the mining industry is undergoing a transformative shift toward sustainability. This change is driven by advancements in battery technologies, improved grid management systems, and the integration of renewable energy sources. The adoption of battery-powered electric vehicles (BEVs) and machinery offers the potential for more efficient, safer, cost-effective, and environmentally sustainable mining operations.

1.1 Background

Growing awareness of climate change has led many industries worldwide to pursue the common goal of reducing carbon-dioxide CO_2 emissions. The mining sector is no exception and is steadily transitioning from diesel-powered machinery and vehicles to their electric counterparts. This shift not only cuts emissions but also improves worker health and safety while enhancing operational efficiency.[1].

The use of electric-powered vehicles is a trend across different industries, as transportation accounts for 21% of the total emissions worldwide[19]. With the advantages of higher energy efficiency, lower maintenance requirements, low pollutant generation, less heat and noise and lower operational cost, electric-power equipment is the candidate to replace internal combustion engines in the mining industry[2].

At the same time, the use of renewable energy sources (RES) like solar and wind has been increasing worldwide due to technological advancements. As a result, more mining sites are implementing this technology as it has the potential to reduce operational cost, reduce greenhouse emissions and improve the energy access in case of remote sites[3]. With this improvements to the mining grid the shift to adoption of BEV is feasible.

1.2 State of the Art

The electrical infrastructure of open-pit mines has undergone significant advancements to meet the increasing energy demands of modern mining operations. Traditionally, these grids have been characterized by a combination of high-voltage substations, medium-voltage distribution networks, and localized low-voltage systems powering critical machinery[9].

Typical load distribution in open-pit mines consists of large industrial consumers such as electric shovels, drills, and haul trucks, which exhibit high peak power demands and intermittent usage patterns. Conveyor belts and dewatering pumps operate more continuously, contributing to the base load of the system, while auxiliary systems, including lighting, ventilation, and processing plants, introduce additional variability[12].

With the integration of battery-electric vehicles (BEVs) and renewable energy sources, the grid structure is evolving to enhance efficiency, reduce emissions, and improve overall system reliability. However, these developments also introduce new challenges, such as grid stability, power quality, and the need for advanced energy storage solutions[10][11].

This thesis presents a comprehensive overview of current grid architectures in open-pit mines and the critical challenges they pose, challenges that are being tackled simultaneously by industry and academia. Particular emphasis is placed on electrically powered drillers, whose rapid-start cycles and induction-motor inrush currents often precipitate significant voltage sags. The study explores advanced methodologies for mitigating these drill-related sags and evaluates the drillers' potential to provide voltage support to the bus to which they are connected

1.2.1 Grid infrastructure in Open Pit mines

Open-pit mining is one of the most widely used surface mining techniques for extracting minerals, including coal, iron ore, copper, and gold. It involves the removal of large amounts of overburden and ore through a stepped excavation, enabling efficient access to mineral deposits near the surface. When comparing this technique to underground mining, open-pit mining offers several advantages, such as lower operational costs, higher production rates, and easier access to larger ore bodies. However, it also presents environmental and logistical challenges, including extensive land disruption, high energy consumption, and the need for continuous infrastructure adaptation as the pit expands[5].
In contrast, underground mining involves complex tunneling systems, ventilation requirements, and strict safety regulations to support excavation stability. While underground mines typically require power distribution via underground cables and transformer stations positioned along haulage levels, open-pit mines rely on a combination of overhead lines, mobile substations, and flexible power distribution networks to meet operational demands[6].

The core operations of an open-pit mine include drilling, blasting, loading, hauling, and mineral processing. Drilling and blasting break the rock into transportable fragments, which are then loaded by electric or diesel-powered shovels onto large haul trucks or conveyors. These transport systems move the material to processing plants or waste dumps, where additional crushing, grinding, and refining processes extract valuable minerals[7].

Each of these operations imposes a significant electrical demand, with peak consumption occurring during loading and transportation activities. Electric shovels and drills, for example, require high peak power levels, often in the range of several megawatts. Additionally, conveyor belt systems, crushers, and grinding mills operate continuously, creating a steady base load in the mine's power system. Auxiliary loads such as lighting, de-watering pumps, and ventilation systems contribute to the overall consumption, necessitating a power distribution network capable of handling dynamic load variations[8].

The electrical grid structure in open-pit mines is designed to accommodate these fluctuating and high-power demands while ensuring operational reliability and safety. Unlike underground mines, where electrical distribution follows a more rigid and confined layout, open-pit mines require a flexible and adaptable power system.
The primary power supply often comes from high-voltage grid connections or on-site power generation, including diesel generators or hybrid energy solutions, voltage is then stepped down via substations and distributed through medium-voltage (typically from 6.6 kV to 36 kV) overhead lines and mobile substations strategically placed around the mining area. This allows power to be relocated as excavation areas shift, preventing infrastructure bottlenecks and minimizing downtime during pit expansions[10][12].

The electrical grid design in open-pit mines is primarily dictated by the operational requirements, load distribution, and the need for flexibility as the mining site evolves. The three most commonly used power distribution topologies in open-pit mining are radial, ring (loop), and mesh (networked) systems. Each topology has its own advantages and limitations, particularly in terms of reliability, scalability, and fault tolerance. The choice of a specific topology depends on factors such as mine size, energy demand, safety requirements, and the economic feasibility of infrastructure deployment[10]. The continuous expansion of open-pit operations requires grid designs that can be adapted dynamically, ensuring efficient power delivery to heavy machinery, processing plants, and auxiliary loads while minimizing downtime and voltage instability[9].

The radial power distribution system is one of the simplest and most cost-effective configurations used in open-pit mines. In this topology, power is transmitted from a central substation and distributed through feeders that extend in a tree-like structure toward different load centers. Each feeder supplies power to a specific area of the mine, with no alternative path in case of a failure. This makes radial systems relatively easy to install, operate, and expand as the pit develops. However, their major drawback is the lack of redundancy. If a fault occurs along a feeder, all downstream equipment loses power until repairs are made. This can lead to significant production losses, particularly in large-scale mining operations where continuous power availability is critical. Voltage drops are also a common issue in radial systems due to long feeder lengths and high load variations, requiring the implementation of voltage regulators and capacitor banks to maintain power quality [11].

To improve reliability, many open-pit mines adopt the ring (loop) power distribution system, where feeders form a closed loop connecting multiple substations and load points. In the event of a fault, power can be rerouted from an alternative path, reducing downtime and improving overall system resilience. This topology provides better voltage stability and is particularly advantageous for medium-sized mines with variable load distributions. Ring networks also facilitate the integration of renewable energy sources, such as solar and wind power, by allowing distributed generation units to be interconnected more effectively. However, the increased complexity and higher initial investment cost compared to radial systems can make this topology less attractive for smaller mining operations. Moreover, protective coordination in ring systems requires advanced relay settings to ensure selective fault isolation without affecting the entire loop [5].

For large-scale open-pit mines with extensive power demands, the mesh (networked) power distribution system offers the highest level of reliability and operational flexibility. This topology consists of multiple interconnected feeders and substations, creating a fully redundant power network. Mesh systems allow for the highest degree of load balancing, minimizing voltage fluctuations and improving the overall power factor. They are particularly beneficial in mines where equipment electrification is a priority, such as those transitioning from diesel-powered haul trucks to battery-electric vehicles (BEVs). Despite their advantages, mesh grids require sophisticated grid control and monitoring systems to manage power flow dynamically. The higher installation and maintenance costs, along with the complexity of protective relay coordination, make mesh topologies less common in mining operations where cost constraints are a primary concern. Nevertheless, with advancements in smart grid technologies and digital substations, mesh systems are becoming more viable for future mining power networks [12].

1.2.2 Electrical Machines in Open Pit mines

Mining is composed by multiple sub-processes in which the total power demanded varies due to the type of electrical load use on the sub-process. Mining demands around 25% of total power having drilling and excavation activities done with electric drillers and shovels[21]. Drillers and Shovels generally use induction motors, and depending on the rated power driller machines can be directly connected to the distribution system[20].

To transport the materials hauling truck or conveyor belts are the available options, in which the load weight and the path inclination define the power consumption. The last stage is the mineral processing sub-process is where the material is reduce in size and separated from waste material using crushing machines, semi-autogenous grinding (SAG) mills and ball mills[20]. Grinding and crushing accounts about 40% and 4% of total power consumed in mine respectively[21].

Drillers and shovels exhibit a non-linear, cyclic load profile in which instantaneous power demand can climb to roughly 1.6 times the average level. For drillers, these peaks coincide with the induction-motor start-up sequence [20]. Shovels are equally critical to mining productivity because they maintain the material flow to downstream processing. Although their large payloads require substantial power, modern drive converters allow a portion of that energy to be regenerated during the loading cycle [22]. Because both machines rely on induction motors that draw large inrush currents, they cannot be started simultaneously on the same feeder without risking unacceptable voltage depressions.

Grinding process requires variable speed drives due to the higher starting torque, where synchronous converters and power electronics are use in this stage. Cycloconverters are the interface between the synchronous machine and the control even though it has low power factor[20].

1.2.3 Challenges currently faced by the mining industry

Traditionally, electrical power systems in the mining industry have been developed through a progressive expansion approach. These incremental expansions proceed in tandem with the growth of mining operations: as the open-pit mine widens and deepens, the electrical network is extended to supply relocated equipment across the various production processes.
This approach proves to be optimal for constant expansions and load addition derived from the mining activities, however it also constrains some characteristics directly related to grid performance, robustness and stability.

The first challenge to be considered relates to the concept of grid strength, this concept quantifies a power system's capacity to maintain stable voltage and frequency under dynamic conditions, particularly with high penetration of inverter-based resources (IBRs)[13].
This measure is mainly characterized by two concepts:

- **Voltage Support Strength**: Determined by the short-circuit ratio (SCR) or weighted short-circuit ratio (WSCR), where (SCR) is defined as it follows SCR = (short-circuit capacity at bus)/(converter rated power).A higher SCR indicates stronger voltage stability[16].
- **Frequency Support Strength**: Measured by system inertia (H, in seconds) and frequency nadir/rocof (rate of change of frequency).A higher inertia and lower rocof signify robust frequency stability, meaning the grid will be able to . Weak grids (low SCR, low inertia) exhibit poor transient response and increased risk of oscillatory instability.

Open-pit mines are often situated in remote locations with limited access to robust utility infrastructure, resulting in weak grid connections marked by high source impedance and low short-circuit capacity. Such conditions introduce a number of technical challenges:

- ***High Impedance and Voltage Regulation Issues***: Long transmission lines (line length $\geq$ 100 km) and inadequate transformer ratings result in significant voltage drops, especially during peak load conditions. For instance, the operation of high-power equipment like electric rope shovels (consuming several MVA) can cause voltage fluctuations that destabilize the grid.

- ***Limited Fault Current Capacity***: Weak grids have low short-circuit capacities, making it difficult to clear faults effectively. This can lead to prolonged outages, as protective devices may not operate reliably under low fault currents.
- ***Integration of Renewable Energy***: With the ongoing green transition and de-carbonization of the mining operations, renewable energy sources (e.g., solar or wind) are being integrated to the grid, however, the intermittent nature of renewables, combined with weak grid infrastructure, results in additional stability challenges[16].

The second challenge considered in the mining industry, correspond to Voltage Stability with a particular interest in a phenomena called: Voltage Sags. Voltage sags are defined by IEEE as a reduction in RMS voltage between 10% and 90% for durations from 8 ms to 1 minute [13]. These phenomena are a prevalent power quality issue in open pit mines due to the disruption in equipment operation and reduction in productivity. The most common but not exclusively causes of Voltage Sags in open pit mines are:

- ***High-Power Motor Startups***: Large motors (700 hp for crushers or 15,000 hp for SAG mills) draw significant inrush currents during startup, causing voltage sags. For example, starting a driller can result in instantaneous voltage dips that trigger protective relays on shovels, halting operations.
- ***Long Cable Runs***: Mobile equipment like shovels and drillers often use long trailing cables, which introduce high impedance and amplify voltage sags.
- ***Faults and Switching Events***: Ground faults, short circuits, or circuit breaker operations can induce sags, particularly in weak grids with limited fault-clearing capacity.

The third challenge presented in this field and project, corresponds to the HARMONIC DISTORTION. Recent development with efficiency goal have introduced VSC and VFD interface for the majority of the electrical machines used in the mine processes. These converters offer several benefits—most notably, they reduce the inrush current drawn by induction machines, enabling smaller cable cross-sections and reducing thermal and mechanical stress on grid assets such as transformers and circuit breakers. The trade-off, however, is the injection of harmonic components into the current waveform. Those harmonics are directly linked to a range of issues, including:

- ***Equipment Heating***: Harmonics can cause additional heating in motors and transformers, reducing their lifespan.powerquality.blog
- ***Resonance Conditions***: Certain harmonic frequencies can resonate with system inductance and capacitance, leading to overvoltages.
- ***Interference with Communication Systems***: Harmonics can interfere with control and communication signals, leading to wrong operation.

Managing harmonic distortion is crucial to maintain power quality and ensure the longevity of electrical equipment.

1.3 Aim

The aim of the project is to model, simulate and analyze a solution implemented in electric drillers to mitigate voltage sags and improve voltage stability in the open-pit grid. To guide the achievement of the research aim, the following questions will be addressed:

- What are the effects on the grid due to the use of high-power machinery?
- What are the available electric machine and drive technologies for drillers operating in open-pit mines?
- What mitigation strategies exist to improve voltage stability?
- To what extent can these available technologies for electrical drillers provide voltage support to the grid?

1.4 Scope

The scope of this thesis project is centered on the electrical drillers utilized by the mining company, specifically exploring their potential to provide voltage support to the power network they are connected to. The primary objective is to evaluate the capability of these drillers, when equipped with standard Active Front End (AFE) configurations, to mitigate voltage sags and contribute to reactive power support. The focus is on quantifying the reactive power compensation in megavolt-amperes reactive (MVAr) and assessing the extent to which these machines can stabilize voltage under varying grid conditions. The proposed system will be modeled and simulated in Matlab/Simulink. Only voltage sags due to the use of high power machinery are considered; other power quality problems are beyond the scope of this thesis.

1.5 Limitations

The scope of this study is limited to the drilling units themselves, focusing exclusively on their capability to provide voltage support without relying on additional grid-side equipment or infrastructure upgrades. No external modifications such as the installation of shunt capacitors, dynamic compensators, or other reactive power devices are considered. Furthermore, the investigation does not address advanced AFE control strategies, maintaining a focus on standard configurations to ensure the research remains within the available time frame. This approach enables a clear assessment of the baseline support capabilities of the drillers, independent of external reinforcement measures or sophisticated control schemes.

2
Theory

The integration of advanced electrical systems into industrial operations requires a clear understanding of the principles that govern performance, reliability, and response to disturbances. In large-scale, energy-intensive settings such as extractive industries, electrical infrastructures face challenging operating conditions that test both design and control strategies. Accurate analysis and effective planning require knowledge of the behavior of the power system, including load-source interactions, the role of electronic power interfaces, and the response of the system to transient events.

This thesis builds its methodology on key principles that affect system behavior in the target application: the mechanisms and impacts of voltage disturbances, the electrical characteristics of open pit mining distribution networks, and the operation of voltage source converters for reactive power control and voltage support. These concepts form the analytical basis for the modeling, simulation, and performance assessment presented in the following sections.

2.1 Induction motors

The three-phase induction motor, particularly the squirrel-cage, is commonly used in industrial applications thanks to its simple construction, which is reliable and robust [28]. It has two components: a stator and a rotor. The stator has windings that, when connected to the supply system, create a rotating magnetic field that rotates at a speed given by the following equation:

$$n_s = \frac{120f}{p} \tag{2.1}$$

Where n_s is the synchronous speed of the motor in rpm, f is the frequency of the grid in hertz, and p is the number of poles of the motor. When rotating magnetic flux cuts the conductors in rotor windings, it induces an electromotive force (EMF) in the windings [29].

As the rotor windings are short-circuited, currents circulate through the rotor windings. As a result, this circulating current tries to counteract the induced EMF. The induced EMF will be countered if the rotating magnetic field and the rotor have the same speed. If this condition is met, there will be no torque production [30]. That is why it is always needed that the rotor speed be less than the synchronous speed. The difference in speed is called the slip and is given by Equation 2.2.

$$s = \frac{n_s - n_r}{n_s} \tag{2.2}$$

where n_r is the rated speed of the motor in rpm.

2.1.1 Motor parameter estimation

In order to analyze the behavior of the induction motor, the simplified equivalent circuit model is used. Figure 2.1 shows the simplified equivalent circuit of the induction motor. The use of this circuit allows for some simplifications that will not introduce significant error.

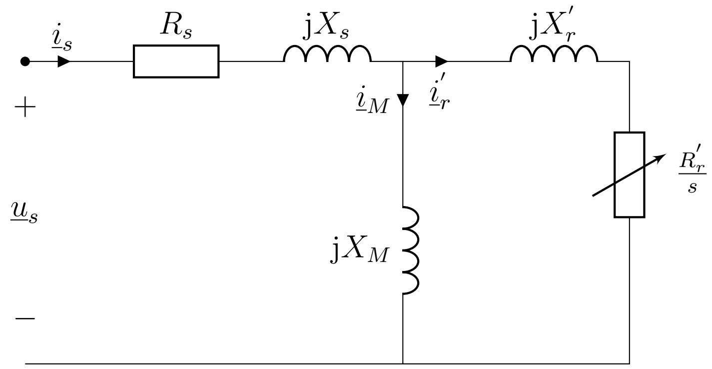

Figure 2.1: Simplified equivalent circuit of induction motor

The elements displayed in the circuit are:

- V_s: Stator voltage
- I_s: Stator current
- R_s: Stator resistance
- X_s: Stator leakage reactance
- X_m: Magnetizing reactance
- X_r': Referred rotor leakage reactance
- I_r': Referred rotor current
- R_r': Referred rotor resistance

Using the rated power and the efficiency of the motor, the input power P_{in} can be found as follows:

$$P_{in} = \frac{P_{out}}{\eta} \tag{2.3}$$

The difference between the input power P_{in} and the output power P_{out} are the total losses in motor:

$$P_{losses} = P_{in} - P_{out} \tag{2.4}$$

An assumption is made here based on the typical ranges of source of losses in induction motors [26], taking the values where the motor present more losses as an edge case. Losses on stator and rotor will be given as follows:

$$P_{Cu1} \approx 0.4(P_{losses}) \tag{2.5}$$

$$P_{Cu2} \approx 0.25(P_{losses}) \tag{2.6}$$

Once the copper losses on stator and rotor are known, the stator and rotor resistances are estimated as:

$$R_s = \frac{P_{Cu1}}{3I^2} \tag{2.7}$$

$$R_r^{'} = \frac{P_{Cu2}}{3I^2} \tag{2.8}$$

Where $R_2^{'}$ is the rotor resistance referred to the stator. Once both stator and rotor resistances are found the equivalent resistance can be calculated as per below equation:

$$R_{eq} = R_s + R_r^{'} \tag{2.9}$$

The next step is to find the equivalent reactance, for this purpose the starting current of the motor I_{st} is used and the equivalent resistance. The equivalent reactance was found as follows:

$$X_{eq} = \sqrt{\left(\frac{V_{ph}}{I_{st}}\right)^2 - R_{eq}^2} \tag{2.10}$$

Where V_{ph} is the phase voltage. Besides this, project the reactance were assumed to have the same value as in NEMA rating A motors, therefore:

$$X_s = X_r^{'} = \frac{X_{eq}}{2} \tag{2.11}$$

The last parameter to find is the magnetizing reactance. However, since the magnetizing current is unknown, another assumption has to be made. The magnetizing current is about 25-50 % due to the air-gap [29], then the magnetizing current is considered as:

$$I_m = 0.3I \tag{2.12}$$

Once the magnetizing current I_m is found then the magnetizing reactance is given by:

$$X_m = \frac{V_{ph}}{I_m} \tag{2.13}$$

The real power transmitted to the air gap P_{ag} from the stator P_i is given by the difference between the input power and the copper losses as shown in Equation 2.14

$$P_{ag} = P_{in} - 3I_s^2 R_s \tag{2.14}$$

If the losses in the core are neglected, there is no element that consumes power but the power dissipated in $R - r^{'}/s$, then the power in the air gap is given by [30]

$$P_{ag} = 3I_s^2 \frac{R_r^{'}}{s} = 3I_s^2 R_s - 3I_s^2 R_r^{'} \frac{(1-s)}{s} \tag{2.15}$$

The power converted into mechanical is the term $I_s^2 R_r^{'} \frac{(1-s)}{s}$, whereas the term $I_s^2 R_s$ represents the rotor copper losses per phase. As a result, mechanical power is obtained by

$$P_{out} = 3I_s^2 R_r^{'} \frac{(1-s)}{s} \tag{2.16}$$

The electromagnetic torque can be determined in terms of mechanical power and rotor speed as

$$T_e = \frac{P_{out}}{\omega_m} \tag{2.17}$$

2.2 Voltage source converters

Voltage source converters (VSC) are semiconductors based converters with the capability of self-commutation. VSC can produce its own AC voltage waveform without the need of the grid. This is achieved thanks to the pulse width modulation technique, in which the magnitude of the signal reference is compared with a triangular waveform [32]. The VSC has the capability of control active and reactive power independently and is able to keep a constant polarity on the DC link [33].

Vector control is the most widely used method used for VSC. In this method the active and reactive currents from the grid are control independent from each other using the rotating dq frame [32]. A balanced three-phase system can be described in space vectors as

$$\vec{v}(t) = \frac{2}{3}(v_a + e^{j\frac{2\pi}{3}} v_b(t) + e^{j\frac{4\pi}{3}} v_c(t)) \tag{2.18}$$

The same space vector described in Equation 2.18 can be expressed by real and complex components as

$$\vec{v}(t) = v_\alpha + j v_\beta \tag{2.19}$$

The transformation can be written also in matrix using the Clarke transform as

$$\begin{bmatrix} v_\alpha \\ v_\beta \\ v_0 \end{bmatrix} = \frac{2}{3} \begin{bmatrix} 1 & -\frac{1}{3} & -\frac{1}{3} \\ 0 & \frac{\sqrt{3}}{2} & -\frac{\sqrt{3}}{2} \\ \frac{1}{2} & \frac{1}{2} & \frac{1}{2} \end{bmatrix} \begin{bmatrix} v_a \\ v_b \\ v_c \end{bmatrix} \tag{2.20}$$

Using the Park transform the signals will be transformed into a DC-value whilst in a steady state. This is achieved by rotating the $\alpha\beta$ reference frame, where θ is the phase angle of the grid voltages, also known as the dq-transform [34] given by

$$v_d + jv_q = (v_\alpha + v_\beta)e^{-j\theta(t)} \tag{2.21}$$

The transformation can be written also in matrix as

$$\begin{bmatrix} v_d \\ v_q \\ v_0 \end{bmatrix} = \begin{bmatrix} cos(\theta(t)) & sin(\theta(t)) & 0 \\ -sin(\theta(t)) & cos(\theta(t)) & 1 \\ 0 & 0 & 1 \end{bmatrix} \begin{bmatrix} v_\alpha \\ v_\beta \\ v_0 \end{bmatrix} \tag{2.22}$$

2.3 Voltage sags

Voltage sags, as defined by IEEE 1159 and IEC 61000-4-30 standards, are short-duration reductions in RMS voltage levels, typically lasting between half a cycle and one minute. These sags are characterized by a decrease in voltage to between 0.1 and 0.9 per unit (p.u.) of the nominal voltage. Identifying a voltage sag involves monitoring the voltage profile and detecting when the voltage dips below a specified threshold for a brief period. [36]

The measurement of voltage sags is governed by parameters such as depth, which indicates how low the voltage drops, and duration, which measures how long the sag persists. These characteristics are critical for assessing the impact of sags on sensitive equipment and for determining compliance with power quality standards. The primary causes of voltage sags at the transmission level include faults such as short circuits, sudden large load changes, and switching operations. At the distribution level, common causes are motor startups, transformer energization, and faults on the distribution lines. [37][36]

In the context of open-pit mines, voltage sags can frequently originate from the large inrush currents associated with starting heavy machinery, such as electric drillers and conveyors. Additionally, frequent switching operations and the variable nature of the loads in mining operations contribute to the occurrence of voltage sags in these environments.[39][40]

2.4 Voltage Support in Power Systems

Voltage support is provided to ensure that voltage levels remain within acceptable limits under various operating conditions for all buses within the power system.

2.4.1 Voltage Stability and Reactive Power Dynamics

Voltage stability refers to the ability of a power system to maintain acceptable voltage levels across all buses under both normal and disturbed conditions [15]. It specifically refers to the system's capability to deliver and sustain adequate reactive power (Q) to meet the continuously varying demands of loads while maintain the voltage profile within desired limits. The incapability of fulfilling the mentioned behavior is know as Voltage instability and it is typically manifested as a continuous and in some cases; slow voltage drop that can eventually result in voltage collapse [14].

Using the two-port power flow equations, one can describe the active (P) and reactive (Q) power delivered to a load in a power system.

$$\begin{aligned} P &= \frac{V_s V_r \sin\delta}{X} \\ Q &= \frac{V_s(V_s - V_r \cos\delta)}{X} \end{aligned} \tag{2.23}$$

where

- P, Q: active and reactive power delivered to the load
- V_s: sending-end voltage
- V_r: receiving-end (load) voltage
- δ: load angle
- X: line reactance

By upfront inspection of 2.23, it can be seen that the reactive component (Q) has a higher order relationship with the voltage of the buses in the power system. Therefore, when performing a sensitivity analysis it is required to inspect the rate of change between these 2 magnitudes; this approach presents the following relationship:

$$\frac{dQ}{dV_s} = \frac{2V_s - V_r \cos\delta}{X}[41] \tag{2.24}$$

When performing a power flow approach, a matrix approach with the Jacobian can be used in order to relate this link in the rate of change between Q and V

$$J = \begin{bmatrix} \frac{\partial P}{\partial \theta} & \frac{\partial P}{\partial V} \\ \frac{\partial Q}{\partial \theta} & \frac{\partial Q}{\partial V} \end{bmatrix} = \begin{bmatrix} J_{P\theta} & J_{PV} \\ J_{Q\theta} & J_{QV} \end{bmatrix} [41] \tag{2.25}$$

The submatrix of interest is:

$$J_{QV} = \frac{\partial Q}{\partial V} \tag{2.26}$$

$$\det(J_{QV}) \neq 0$$

In steady-state voltage stability analysis, the singularity of the reduced Jacobian submatrix $J_{QV} = \frac{\partial Q}{\partial V}$ (i.e., $\det(J_{QV}) = 0$) indicates that the system has reached its maximum loadability limit, commonly represented by the "nose point" on a P–V curve.
This point marks a *necessary condition* for voltage instability in the static framework, as it corresponds to the loss of a unique power flow solution beyond which the system cannot sustain additional load without a voltage collapse.

However, it is not a sufficient condition, as instability may occur earlier due to reactive power limits, load dynamics, or control interactions [14][41].

The previous mathematical approach displays the intrinsic relationship between the reactive power in a power system and the buses of it, one can infer the need for a proper Q management with the objective of ensuring voltage stability within the system.

2.4.2 Mechanism to provide Voltage Support

In order to ensure the voltage stability in a power system, there are different strategies and devices that can offer a direct reactive power management flowing in the systems under different load conditions and contingencies. The devices can be categorized in 2 sets, static and dynamic.

2.4.2.1 Static Reactive Compensation

Static reactive compensation is a type of compensation provided by passive elements that provides or absorbs reactive power to or from the grid. Example of static compensating devices:

- **Shunt Capacitor Banks**: Connected in parallel, they provide leading reactive power and are mainly used to raise voltage level and are commonly deployed locally.
- **Shunt Reactors**: Connected in parallel, they absorb reactive power from the grid and their main used is to reduce the voltage level at the particular bus.

2.4.2.2 Dynamic Reactive Compensation

Dynamic reactive compensation is a type of compensation that can adapt and change to the different loading and power flow conditions that a system is experiencing. This strategy is able to achieve this by exploiting the controllable capability of some power electronics like thyristors and IGBTS, devices that can block or allow the flow of current through them when desired by a controllable triggering signal. The main known devices of dynamic compensation are:

- **Static Var Compensator (SVC)**: Is a device which combines a Reactor and Capacitor within a thyristor controllable interface in order to provide or absorb the required reactive power.
- **STATCOM**: This device uses a power electronics interface (IGBT) to provide the needed compensation (absorption or injection), its response its much faster and reliable in different scenarios.
- **Synchronous Condenser**: This consist of an electrical generator that operates without mechanical prime mover and is able to provide or absorb reactive current depending on the excitation conditions.

3

Modelling of Mining Machines and Distribution Grid

This degree project encompass investigation and proposal for integration of voltage support functionalities into electric drillers employing Active Front-End (AFE) converters within mining industry. This with the sole target to counteract voltage sags induced by inrush currents during induction motor startups, fault events and chaging loading conditions.

The methodology uses a systematic approach, beginning with an analysis of advanced motor control and topological configurations of electrical distribution networks in mining operations. Subsequently, detailed Simulink models are developed and calibrated to emulate the dynamic behavior of the system. These models are subjected to simulations encompassing a spectrum of loading scenarios and fault conditions to assess transient and steady-state performance.

The final phase involves the design and implementation of voltage support mechanisms making use of the AFE control strategies and testing of this solution under varying grid conditions while comparing the results to the ones obtained with the traditional approach.

3.1 Overview of current industry strategies, research and findings

This section involves a thorough review of current industry practices and technological advancements in the control of induction machines and the design and deployment of electrical grids. The focus is placed on identifying the technical implications, key operational advantages, and potential challenges associated with these developments.

The insights gathered from this review serve as the foundation for defining the electrical network topology of the proposed system. Additionally, they inform the selection of suitable induction motor configurations for each machine integrated into the overall power system.

3.1.1 Electric motor and drive system for drilling machines

Drillers and shovels are essential equipment in the mining process, as they supply the raw material that must be moved and processed to maximize mine production and efficiency. Any malfunction or downtime of these machines can significantly impact the mine's profitability, making it crucial to ensure their reliable operation.

Drilling rigs generally rely on squirrel-cage induction motors because their rugged construction and minimal maintenance align well with the abrasive, dust-laden mining environment. For medium-voltage ratings, these motors are typically energized Direct-On-Line (DOL), i.e., connected straight to the grid without soft-starting. At start-up, however, an induction motor behaves almost like a short circuit, drawing inrush currents five to seven times its rated value—most of which is reactive—while the air-gap flux builds and the rotor accelerates to synchronous speed. This MVAr surge depresses the local bus voltage, producing voltage sags that can compromise neighboring equipment and power-quality compliance.

In open-pit mining operations, this issue is particularly critical because shovels, which are often connected to the same electrical bus as the drillers, are highly sensitive to power quality disturbances when using electrical drives [7]. Drive sensitivity to voltage sags increases when the rated voltage is close to 90 % of the rated voltage at the point of common coupling (PCC) [46]. As a result, voltage sags originating from driller startups can directly disrupt shovel operation, this can lead to a considerable production loss, specially when mining materials are precious [8].

To address these challenges, several mitigation strategies are available, each with its own advantages and limitations. The choice of method depends on the specific operational constraints and requirements of the mine. Table 3.1 provides a comparative overview of some commonly used solutions.

Table 3.1: Motor and drive systems comparison for Induction motors

Electric motor and drive systems				
Motor/Drive	**Inrush Current**	**Power Factor**	**Harmonics Emission**	**Advantages / Disadvantages**
Direct-on-Line (DoL)	No mitigation mechanism; motor draws high amount of current	Low power factor around 0.8 - 0.85, possible steady state compensation using shunt capacitor	It does not produce harmonics, but does not mitigate them	Simple, cheapest / High inrush current that produces voltage sags
Induction motor with Soft Starter	Controls thyristor firing angle to reduce voltage and current	Same as DOL during normal operation	Thyristor switching distorts current waveform during start	Reduces inrush and sag via controlled voltage ramp / No harmonic mitigation; only used during starting

Continues on next page

Electric motor and drive systems (cont.)				
Motor/Drive	**Inrush Current**	**Power Factor**	**Harmonics Emission**	**Advantages / Disadvantages**
Inverter drive system with diode-front-end	Controls torque/flux current components to cut starting current	Power factor about to 0.95 [48], possible shunt capacitor compensation	Diode rectification and valve switching introduce harmonics with frequency factor of $6k \pm 1$ [47] / high total harmonic distortion content	Limits starting current by reducing voltage mitigating sags / Need filtering to mitigate harmonics produced
Inverter drive system with active-front-end	FOC control regulates torque/flux currents, minimizing inrush	It can regulate reactive power and power factor at the grid side to support grid voltage	PWM control keeps supply current near-sinusoidal and harmonic content is about 5 % [49]	Controls voltage/speed; lowers inrush current and mitigates voltage sag / Generates high-frequency harmonics

3.1.2 Electrical grid in open pit mines

This phase of the project concentrates on open-pit-mine electrical networks and develops a representative benchmark model that will serve as the test platform for the proposed mitigation strategy. Its primary objective is to deliver a rigorous characterization of the topology, loading conditions, and operating practices of open-pit grids currently in service. The scope of this research is the following:

- Medium Voltage (13.8 kV) grid composition.
- Medium Voltage grid topology
- Loads composition and distribution around MV grid.
- Transforming centers distribution around MV grid.
- Reactive compensating mechanisms

Out of the scope of this research is:

- Medium Voltage (33 kV) grid feeder.
- Transmission Level feeder topology.
- Specific induction motors technicalities.
- Deeper control strategies

3.1.2.1 Research targets

The main goal is to provide a characterization of the medium voltage grid typically built for open pit mines, both in qualitative and quantitative specifications for model construction.

The specific milestones for this research are

- Determine the topology for the 13.8 kV, select either radial or mesh.
- Define viable sizes for loads rating based on the existing open pit mines.
- Define medium voltage grid power lines, providing length, rating capacity, design, conductor selection and compensating mechanism if needed.
- Define accurate strength rating for grid feeder, provide SCA capacity, X/R ratio and Isc if possible.
- Explore and gather different grid strength ratio currently existing in the world to have as test scenario.

3.1.2.2 Revised Sources

The information was gathered from several sources, a categorization can is presented below:

- Academic reports on the IEEE database focused on the electrical specifications of the mine power system for different applications. [22][10][20][22][11]
- Mining companies technical reports regarding their mining operation.[4]
- Mining companies and components manufacturers white papers presenting product solutions and case study for their implementations. [12][26]
- Power components (Transformers, ASCR cables) manufactures datasheet presenting electrical detailed specifications.
- Electrical Standards for grid development IEC 60826

3.1.2.3 Required Grid Information

The relevant parameters obtained from the literature review are presented in the following table:

Table 3.2: Grid Characterization Parameters

Item	Parameter	Description
1	Topology	Are grids mostly developed following a radial or mesh structure?
2	Short Circuit Capacity (MVA)	What are the typical short circuit capacities?
3	X/R ratio	Insight into how inductive the grid is and expectations about behavior during voltage drops.
4	# Buses	How many buses typically compose the used grid?
5	Transformer Parameters	Required parameters such as impedance, leakage reactance, and magnetizing reactance.

Continues on next page

Grid Characterization Parameters (cont.)		
Item	**Parameter**	**Description**
6	MV Line Disposition and Size	Typical power line capacities, commonly selected cable sizes, and phase dispositions.
7	Q Compensators Allocation and Sizing	Typical allocation of capacitors and sizing at different busbars.
8	Loading Profile Distribution	Typical MVA loading per busbar.

3.1.2.4 Selected grid characterization parameters

After gathering information and typical data for the stipulated parameters presented in Table 3.3, the following power systems is built incorporating the information.

Table 3.3: Grid Characterization Parameters

Item	**Parameter**	**Description**
1	Topology	The power system follows a radial layout: six main buses linked to the feeder. Pit-located buses are supplied via intermediate buses and overhead lines.
2	Short Circuit Capacity (MVA)	Range for typical operation is 450–250 MVA. Study range: [400–80] MVA.
3	X/R Ratio	Common values range between 15 and 30.
4	Number of Buses	Six MV buses are included, consistent with 6–10 bus systems in similar cases.
5	Transformer Parameters	Ratings used: 50, 10, and 5 MVA. Parameters obtained from equipment datasheets.
6	MV Line Configuration	All lines use the same conductor type and layout to avoid transfer constraints.
7	Reactive Compensation	Shunt capacitors per bus, sized up to 25% of the active power demand.
8	Load Profile	Defined using EPIROC equipment ratings and operational guidelines.

3.2 Power system and Machines models

3.2.1 Electrical Machines modeling

High power induction machines are considered key elements of the open pit mine. The core activities of production are related to these machines, thanks to their efficiency and resilience to harsh conditions. Based on the literature review, the rated power of the machinery of the grid was defined [35], then commercial induction motor catalog was used [27] to estimate the motor parameters utilized in the modeling. Estimation was conducted instead of locked-rotor and no-load test due to the lack of physical motor to conduct such tests.

The machine parameters were estimated using power losses relations [42] and assumptions to streamline the modeling process. This approach aligns with the scope of the project, which prioritizes the analysis of voltage stability in the power system rather than detailed parameter identification of individual components. The nameplate and catalog data used as the basis for parameter estimation of the induction motor are presented in: Table 3.4.

Table 3.4: Induction Motor Parameters from catalog [27]

Parameter	**Driller**	**Shovel**	**Aggregated Load**
Rated power: P_r	500 kW	2 MW	3 MW
Rotor speed: n_r	1484 rpm	1490 rpm	1491 rpm
Rated voltage: V_r	690 V	690 V	13.8 kV
Rated current: I_r	504 A	1941 A	169 A
Rated frequency: f_r	50 Hz	50 Hz	50 Hz
Pole pairs: p	2	2	2
Efficiency: η	94.3 %	95.8 %	96.8 %
Power Factor: PF	0.88	0.90	0.91
Starting current: I_A/I_r	6.2	6.3	6.4
Starting torque: T_A/T_r	0.9	0.7	0.7
Max. torque: T_k/T_M	2.3	2.5	2.7
Inertia: J	23 $kg\,m^2$	80 $kg\,m^2$	205 $kg\,m^2$

The motor parameters of a 500 kW driller machine were estimated using the approach described in Section 2.1. The estimated parameters can be found in Table 3.5.

Table 3.5: 500 kW Driller Motor estimated parameters

Parameters	**Values**
Stator resistance: R_s	0.01 Ω
Referred rotor resistance: $R_r^{'}$	0.01 Ω
Stator leakage reactance: X_s	0.06 Ω
Referred rotor leakage reactance: $X_r^{'}$	0.06 Ω
Magnetizing reactance: X_m	2.1 Ω

To validate the estimation of the parameters, the motor is simulated using Simulink where the parameters are introduced in a motor block and then the technical catalog values will be contrast against the values obtained with the simulation. In Table 3.6 are shown the results with the respective error.

Table 3.6: Comparison between catalog and simulation values for 500 kW induction motor

Parameter	Technical Catalog	Simulation	Deviation
Rated power: P_r	500 kW	509.5 kW	1.9 %
Rotor speed: n_r	1484 rpm	1482 rpm	0.13 %
Rated current: I_r	504 A	485.33 A	3.7 %
Efficiency: η	94.3 %	95.8 %	1.5 %
Power Factor: PF	0.88	0.87	1.1 %
Starting current: I_A/I_r	6.2	6.29	1.4 %
Starting torque: T_A/T_r	0.9	0.81	10 %
Nominal torque: T_k/T_M	3183.1 Nm	3199 Nm	0.5 %
Max. torque: T_k/T_M	2.3	2.26	1.7 %

Overall, the results of the motor simulation with the estimated parameters based on the technical catalog present a deviation equal or less than 10 %. The starting torque having a deviation of 10% is the highest deviation among all parameters, while the remaining parameters shows a deviation less than 5%. As the results of the simulation show a high level of accuracy respect the technical catalog, the model can be reckoned as validated and used in the simulation of the grid model.

The same procedure was used to calculate the motor parameters for induction motors of 2 MW and 3 MW to be used in the shovel and aggregated loads of the model. The results were not as accurate as those of the 500 kW induction motor, therefore another strategy was used. It was decided to use the parameter estimation tool of the asynchronous machine block in Simulink to obtain the motor parameters. This decision was motivated by the need to have an accurate voltage and current measurement, as well as power consumption, in the different buses of the grid. To be able to use the estimated parameters offered by the tool, the motor configuration had to be configured as double squirrel cage. In Table 3.7 the estimated parameters for the induction motors used in shovel and aggregated load models are shown.

Table 3.7: Induction motor estimated parameters for shovel and aggregated loads

Parameter	**2 MW motor values**	**3 MW motor values**
Stator resistance: R_s	7.989 e-7 Ω	4.790 e-7 Ω
Stator leakage reactance: X_s	0.0241 Ω	0.0129 Ω
Referred rotor resistance 1: R'_{r1}	0.001717 Ω	0.0011 Ω
Referred rotor leakage reactance 1: X'_{r1}	0.0368 Ω	0.0331 Ω
Referred rotor resistance 2: R'_{r2}	0.0126 Ω	0.0036 Ω
Referred rotor leakage reactance 2: X'_{r2}	0.0241 Ω	0.0129 Ω
Magnetizing reactance: X_m	1.616 Ω	0.5984 Ω

3.2.2 AFE motor drive design

The active front-end drive model used implements sensorless rotor field-oriented control (FOC) method [43][44][45] to control the induction motor and reactive control in the rectifier [23]. In FOC method, the torque and flux are controlled independently, similar to the control of a DC motor. Compared to traditional scalar control methods, FOC offers significantly improved dynamic performance and transient response.

Due to the lack of a physical motor test data, the motor parameters used in the model were estimated, which reduces the accuracy of the simulation. As a result, the original sensorless control approach could not be directly applied. To address this limitation, an observer block was implemented to estimate the motor's flux and speed. Figure 3.1 shows the block diagram of the FOC control for the induction motor. Estimated flux and speed values are compared with the reference torque and flux values. The resulting error signals are processed by PI controllers, which generate the reference currents in the dq frame.

These reference currents are then compared with the measured dq currents, and the resulting error is again fed into PI controllers to compute the reference dq voltages. These voltages are transformed back to the three-phase (abc) system through the inverse Park and Clarke transformations, producing the three-phase voltage references [25]. These are used by the PWM controller, which drives the inverter to control the motor accordingly.

On the other hand, the control system for the rectifier includes inner current control loops for the d-q axis currents, and an outer voltage control loop that regulates the DC bus voltage. The measured DC voltage is compared with a reference value, and the resulting error is processed by a PI controller, which generates the reference i_d current. Since the objective is to transmit only active power, the reference value for i_q is set to zero. This zero reference is compared with the measured i_q current, and the error is again passed through a PI controller to regulate the current accordingly.

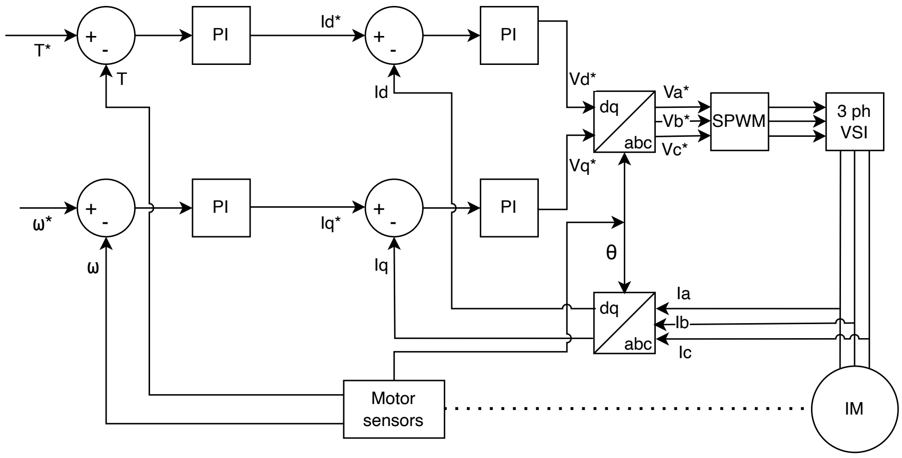

Figure 3.1: Flux oriented control for induction motor

The active front end rectifier control has to inner control loops for currents in d-q frame and an outer loop to control the DC voltage. The inner loops are configured to provide maximum active power transfer, which means that the reference for the q-component of the current is normally set to zero. Figure 3.2 shows the control block diagram of the AFE. To enable the drive system to provide voltage support capabilities, the control of the Active Front End (AFE) rectifier was modified. When this support feature is active, the controller monitors the DC bus voltage, and if it drops below a predefined threshold, the AFE begins to inject reactive current into the grid. This injection is synchronized using the phase angle provided by the PLL, helping to stabilize the system voltage during disturbances.

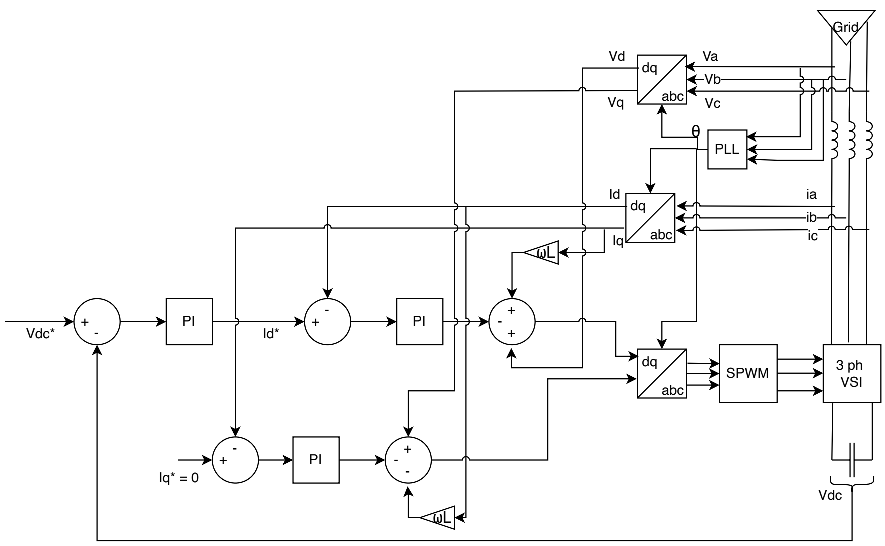

Figure 3.2: AFE control diagram

To achieve the grid voltage regulation, an outer voltage control loop of the AFE converter is added. It calculates the error between the bus target voltage and the measured voltage. This error is passed through a PI controller which provides the reactive current reference I_q^*. This change will affect the power factor of the AFE as the I_q current is no longer maintained to zero, but will enable the capability to provide reactive power to the grid. Reactive current can be both injected to and absorbed from the grid. Figure 3.3 shows the modified AFE control diagram.

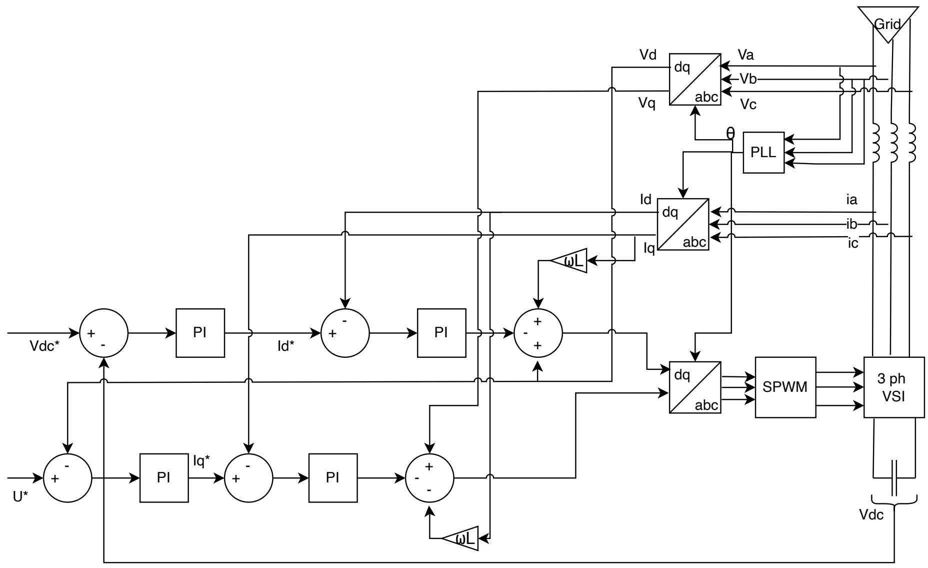

Figure 3.3: AFE control diagram

3.2.3 Description of mining distribution grid

The power system model developed for this study was modified based on the system described in [Jeronen et al., 2021] [12]. Rated powers and spatial placement of the principal loads (drill-rig drives, pumping and shovel units) were refined using nameplate data and application notes supplied by Epiroc and revised literature, ensuring that the simulated equipment reflects the manufacturer's current production portfolio and current industry practices. [31][4]

The power system is presented in the following single line diagram :

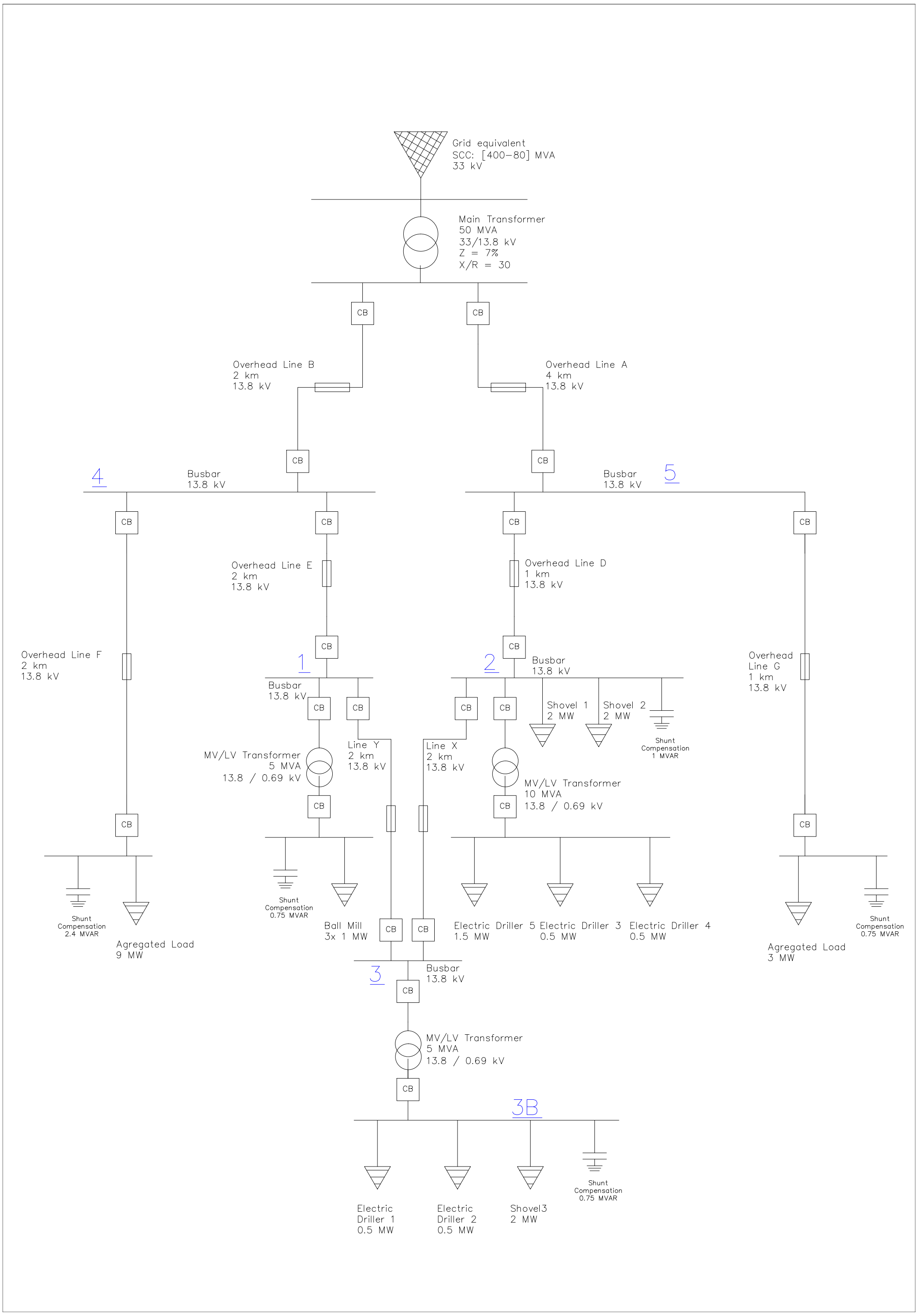

Figure 3.4: Single Line Diagram for proposed power system

The power system is supplied by a primary transformer rated at 50 MVA that energizes two radial, medium-voltage main buses (Bus 4 and Bus 5). Each main bus feeds a dedicated 13.8 kV secondary bus (Bus 1 and Bus 2, respectively), which, in turn, is equipped with a step-down transformer bank (13.8 /0.7 kV) for low-voltage distribution to process loads. From both secondary buses, twin parallel 13.8 kV feeders are routed to Bus 3, the electrically most remote node located at the greatest pit depth.

Due to its long feeder impedance and distance from the stiff source, Bus 3 constitutes the limiting node for steady-state voltage stability and is the location most prone to voltage drop and flicker during motor-starting or contingency events; consequently, it represents the critical bus to focus on for reactive-power support and voltage-regulation studies within the mine's internal grid.

Buses 1, 2, and 3 constitute the core electrical infrastructure of the pit, serving as the primary nodes for all loads and processes within the open-pit mining operation. In contrast, Buses 4 and 5 are associated with the external surrounding area, providing a clear differentiation between the internal and peripheral electrical distribution zones. For modeling purposes, the pit's operational loads have been represented as induction machines of specific rated capacities, ensuring a realistic simulation of the load dynamics.

Furthermore, each of these pit buses (Buses 1, 2, and 3) has been equipped with reactive power compensation systems, which improve the power factor at the bus. The reactive compensation had been carefully sized to not exceed 25% of the active power demand of the bus, thus optimizing voltage stability.

Additional technical specifications and parameters are detailed in Table 3.9, which provides a comprehensive overview of the reactive support and load characteristics for each bus.

The corresponding parameters for the transformers, power lines, shunt compensators used in the proposed model are detailed in the following tables:

Table 3.8: Transformer Specifications

Trf	Rating (MVA)	Freq (Hz)	V1 (kV)	V2 (kV)	Prim Wind Res (p.u.)	Sec Wind Res (p.u.)	Prim Leak React (p.u.)	Sec Leak React (p.u.)	Zero Seq React (p.u.)
A	50	50	33	13.8	2.7978E-03	4.8926E-04	0.034972	0.034972	0
B	10	50	13.8	0.7	4.3458E-03	1.12E-05	0.03368	0.03368	0.10104
C	5	50	13.8	0.7	5.5414E-03	1.43E-05	0.033636	0.033636	0.10091

Table 3.9: Shunt Capacitor Parameters

Shunt Compensator Location	**Configuration**	**Capacitor Size (µF)**	**Rated Reactive Power (MVAR)**
Bus 1	Y Configuration	4880	0.85
Bus 2	Y Configuration	15	1.8
Bus 3	Delta Configuration	1600	0.85
Bus 4	Y Configuration	38.4	2.631
Bus 5	Y Configuration	12.5	0.85

Table 3.10: Overhead Line Parameters

Element	**Length (km)**	**Resistance (ohms/km)**	**Inductance (mH/km)**	**Capacitance (µF/km)**	**Observation**	**MATLAB Model**
Overhead Line A	4	0.069555	1.3183	0.0087679	ACSR Drake 795 kcmil 26 Strands 1 conductor /phase	PI Model
Overhead Line B	2	0.069555	1.3183	0.0087679		
Overhead Line D	1	0.069555	1.3183	0.0087679		
Overhead Line E	2	0.069555	1.3183	0.0087679		
Overhead Line F	2	0.069555	1.3183	0.0087679		
Overhead Line G	1	0.069555	1.3183	0.0087679		
Overhead Line X	2	0.069555	1.3183	0.0087679		
Overhead Line Y	2	0.069555	1.3183	0.0087679		

3.3 Simulation

Once the power system model was fully implemented—incorporating all relevant components such as induction motors, transmission lines, transformers, and associated parameters—the simulation was conducted within the MATLAB Simulink environment, utilizing the Simscape Electrical toolbox. The simulation process began with a comprehensive verification of all input data to ensure accuracy and reliability.

Table Table 3.11 summarizes each step of the simulation and the corresponding operational states of the system. The dynamic load flow analysis was then executed, taking into account the exchanges of active and reactive power, as well as the resulting voltage profiles and other critical variables.

Table 3.11: Sequence of system events

Second	**Action**
12	Magnetization of driller 1
17	Driller 1 goes to max load
19	Magnetization of driller 2
23	Driller 2 goes to max load
30	End of simulation

Special attention was given to Bus 2 and Bus 3, identified as the most electrically distant points to the main grid within the hypothetical open-pit mine scenario. These buses represent the furthest nodes from the main feeder and the point of common coupling (PCC), making them the most susceptible to voltage deviations and, therefore, key focal points in the analysis.
The entire system is first solved in load-flow to confirm that the pre-disturbance steady state of the loads is within acceptable operating limits and then initialize the dynamic simulation. All target interest drillers remain de-energised during this phase to ensure that any subsequent voltage excursions can be attributed exclusively to their energisation sequence.

Once steady-state conditions are confirmed, each driller motor is energized individually. During the magnetizing inrush interval, bus voltages are sampled at 1 kHz so that sag depth, duration and the post-sag steady-state deviation can be extracted with high temporal fidelity. After the stator flux has stabilized, a torque reference is imposed to emulate the mechanical drilling load, thereby transitioning the motor from no-load operation to loaded operation. The procedure is repeated for every driller, with the cumulative number of motors directly influencing the frequency and severity of sag events captured in the waveform record.

3.3.1 Test Scenarios Conditions

In the simulation framework, three primary test scenarios were considered to evaluate the system's performance under varying conditions.

3.3.1.1 First Scenario: Baseline with both Electric Drill rigs under DOL

The first scenario represents the baseline, reflecting the common industry practice where mining companies utilize Direct-On-Line (DOL) starters for their machinery. This scenario serves as the reference point for comparison. In this baseline scenario, the simulation was conducted by sweeping through different values of grid strength, defined by the short-circuit capacity at the Point of Common Coupling (PCC), to assess the impact of grid strength on voltage sag characteristics and the overall system response.

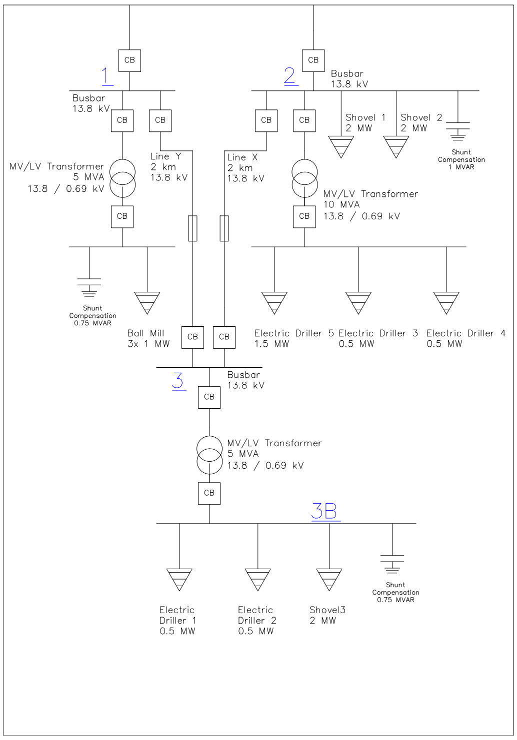

Bus	Name	Pwr	Qty
4	Agg. load L	9 MW	1
5	Agg. load R	3 MW	1
3B	Shovel	2 MW	1
3B	Driller 1	0.5 MW	1
3B	Driller 2	0.5 MW	1
2	Shovel	2 MW	1

Table 3.12: Load allocation and schematic overview. Left: Load distribution schematic. Right: Equipment allocation per bus.

3.3.1.2 Second Scenario: Both Electric Drill rigs under AFE -Unity PF

The second scenario mirrors the first in terms of the event sequence and grid strength variations, but with one key modification: the drillers are equipped with Active Front End (AFE) converters. The integration of AFE technology aims to reduce the reactive power demand of the motors and thereby minimize their impact on the grid. This scenario allows for a direct comparison with the DOL configuration to determine the effectiveness of AFE in mitigating voltage sags and improving voltage stability.

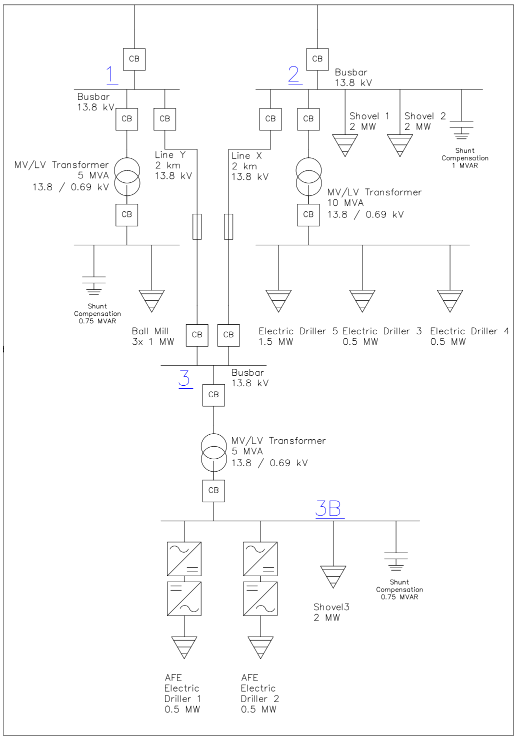

Bus	Name	Pwr	Qty
4	Agg. load L	9 MW	1
5	Agg. load R	3 MW	1
3B	Shovel	2 MW	1
3B	Driller 1	0.5 MW	1
3B	Driller 2	0.5 MW	1
2	Shovel	2 MW	1

Table 3.13: Load allocation and schematic overview. Left: Load distribution schematic. Right: Equipment allocation per bus.

3.3.1.3 Third Scenario: One electric drill rig equipped with AFE + Q Support

The third scenario builds on the second by enabling the compensatory functionality of one of the AFE-equipped drillers. This scenario explores the potential of the AFE driller to provide reactive power support, thus compensating for the reactive power demands of other DOL-connected machines. The objective is to quantify the extent to which the AFE driller can mitigate voltage sags and improve steady-state voltage conditions, as well as determine the number of DOL machines that can be supported under this configuration.

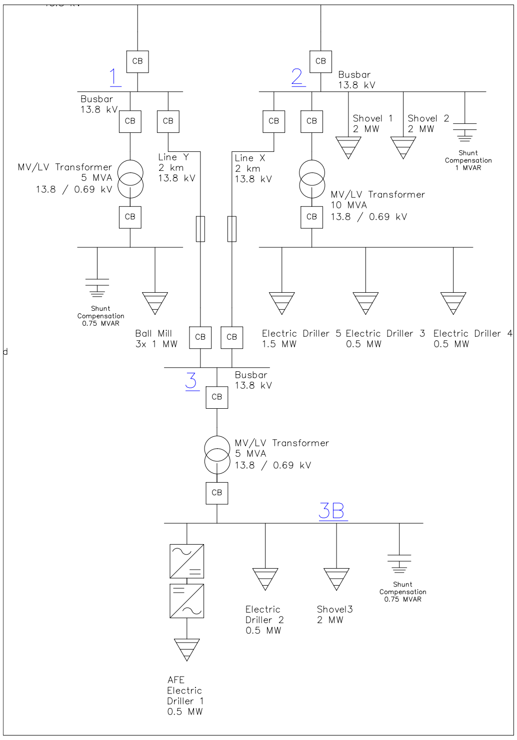

Bus	Name	Power	Qty	Comp.
4	Agg. load left	9 MW	1	0
5	Agg. load right	3 MW	1	0
3B	Shovel	2 MW	1	0
3B	Driller 2	0.5 MW	1	0
2	Shovel	2 MW	1	0
3B	Driller 1	0.5 MW	1	500 kVAr

Table 3.14: Load allocation and schematic overview. Left: Load distribution schematic. Right: Equipment allocation with compensation.

For each of these scenarios, the simulations included a systematic variation of the short-circuit capacity at the PCC to observe how voltage sags evolve and to understand the mitigation capacity of the theoretical AFE driller under different grid conditions. A summary table is presented below

Table 3.15: Simulation Test Scenarios and Expected Outcomes

#	Scenario	Configuration Overview	Simulation Objectives	Key Metrics / Expected Outcomes
1	Baseline (DOL)	Two MV drill-rig induction motors at **Bus 3** started via **Direct-On-Line** (DOL) method; no supplemental reactive-power devices.	Benchmark the network's inherent immunity to voltage sags while sweeping the grid-strength ratio (GSR): $\mathrm{GSR} = \frac{S_{\mathrm{SC,PCC}}}{S_{\mathrm{TX}}}$	• Sag depth and duration at Buses 2 and 3 • GSR threshold where IEEE Std 1159 limits are breached • Baseline MVAr demand

Continues on next page

Simulation Test Scenarios and Expected Outcomes (cont.)				
#	**Scenario**	**Configuration Overview**	**Simulation Objectives**	**Key Metrics / Expected Outcomes**
2	AFE — Unity PF	Same topology, but both drillers retrofitted with **Active Front End (AFE)** drives commanded to unity power factor ($Q \approx 0$).	Quantify how AFE drives: (i) attenuate sag depth/duration, and (ii) reduce the reactive burden, over the identical GSR sweep	• % sag reduction vs. Scenario 1 • Net MVAr decrease at PCC
3	AFE + Q Support	Driller 2 remains with DOL control mechanism; Driller 1 is equipped with AFE with **dynamic Q-support** (capacitive MVAr injection).	Evaluate the AFE's capability to stabilise voltage under weak-grid conditions and determine the *maximum number of additional DOL machines* that can be supported	• Sag depth/duration with Q-support enabled • Steady-state $V \geq 0.95$ p.u. • DOL-machine support capacity at each GSR step

3.4 Results adquiring and acceptance criteria

In the process of obtaining results, particular attention was directed towards the voltage profiles at each bus within the system. The evaluation criterion for voltage levels was set within a tolerance band of ±10% around the nominal value of 1.0 per unit (p.u.), thereby defining an acceptable operating range between 0.9 and 1.1 p.u. Any voltage measurements falling below this threshold were flagged as significant and classified as voltage sags in accordance with the IEEE1564 or IEC61000-4-11 standards.

Depending on the depth and duration of these voltage sags, the performance of the two connection schemes—Direct-On-Line (DOL) and Active Front End (AFE)—was cataloged and subsequently compared. Additionally, the study focused on the reactive power demand and consumption at each node where the motors were connected. This allowed for a thorough assessment of the impact and potential benefits of transitioning from a traditional DOL configuration to an AFE scheme.

Furthermore, measurements included not only the active and reactive power consumption of the drillers and their respective buses, but also the active and reactive power supplied by the main feeder. his dual focus allowed for a comprehensive assessment of how transitioning from DOL to AFE configurations could optimize both voltage stability and reactive power management.

The table below summarizes the key variables and parameters monitored during the analysis:

Table 3.16: Monitored Variables and Acceptance Criteria

Parameter	**Description**	**Range / Criterion**
Voltage (p.u.)	RMS voltage magnitude at each bus, expressed in per unit.	$0.9 \leq V \leq 1.1$ p.u.
Voltage-sag depth	Maximum deviation of bus voltage below 0.9 p.u. during a sag event.	IEEE Std 1159-2019 limits[1]
Voltage-sag duration	Time interval for which $V < 0.9$ p.u. persists.	IEEE Std 1159-2019 classification
Reactive power demand, Q	Total reactive power absorbed by motors and local loads at each bus.	Monitored (comparison DOL vs. AFE)
Active power, P	Total real power absorbed by motors and local loads at each bus.	Monitored (comparison DOL vs. AFE)
Feeder supply (P, Q)	Active and reactive power delivered by the main feeder to the pit network.	Monitored to quantify overall impact

The following diagram shows the measured variables taken for this project:

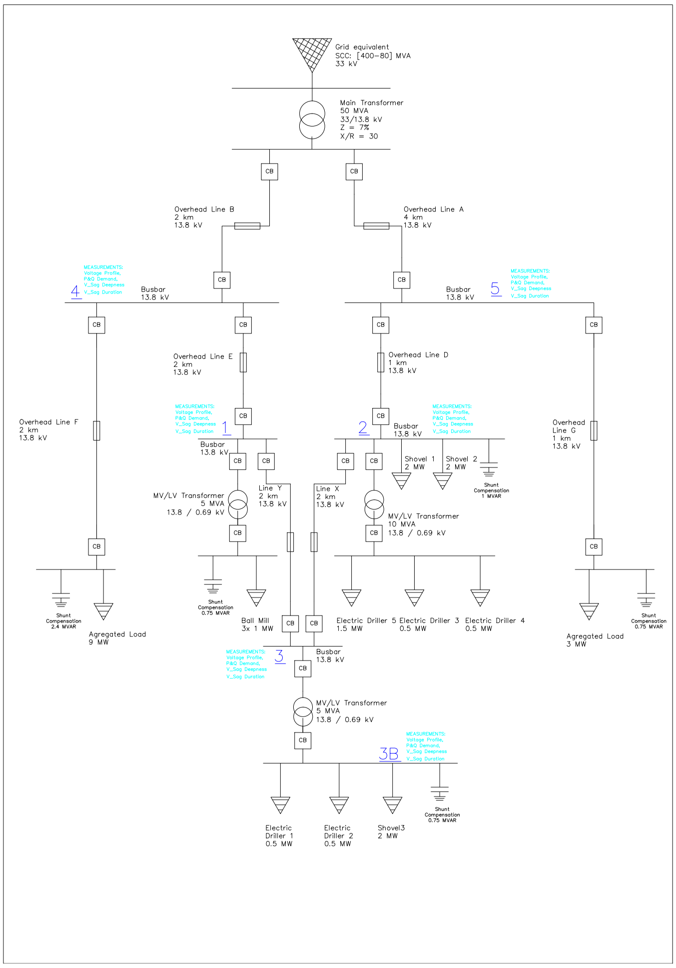

Figure 3.5: SLD with location for measured variables

4

Results and Discussion

This Results chapter synthesises the numerical and waveform data obtained from the MATLAB Simscape Electrical ^{TM} simulations, translating the test plan into quantitative evidence. It begins by validating that all buses operate within the range 0.9–1.1 p.u prescribide in IEC60038 [50]. steady-state envelope, after which it dissects the voltage-sag events recorded at the two electrically weakest nodes—Bus 2 and Bus 3—classifying their depth and duration in accordance with IEEE Std 1159-2019.

The analysis then compares the Direct-On-Line (DOL) and Active Front End (AFE) drive configurations under both full-load and duty-cycle scenarios, highlighting the impact of each scheme on bus-voltage recovery and feeder loading as the grid strength variates due to short circuit capacity reduction. Finally, the chapter integrates active- and reactive-power trends at the driller terminals to demonstrate how AFE-based torque control can mitigate the reactive burden imposed by large drill-rig starts while preserving overall system stability and contributing to this characteristic, providing a differentiated factor from other solutions.

4.1 Driller with DOL as voltage sag source

In Figure 4.1, we illustrate the anticipated dynamic behavior of the system's key events. The simulation spans a total of 30 seconds, encompassing the full energization sequence of the network and, more specifically, the sequential startup of the two drillers. Initially, the system operates with the existing Direct-On-Line (DOL) configuration, serving as the baseline for comparative analysis.

At the 12-second mark, the event sequence begins: the first driller undergoes magnetization, followed by the application of torque. Subsequently, the second driller is energized in a similar manner, culminating in the system reaching a new steady-state condition. This progression allows us to observe and confirm the occurrence of voltage sags induced by the inrush currents and load application of each driller.

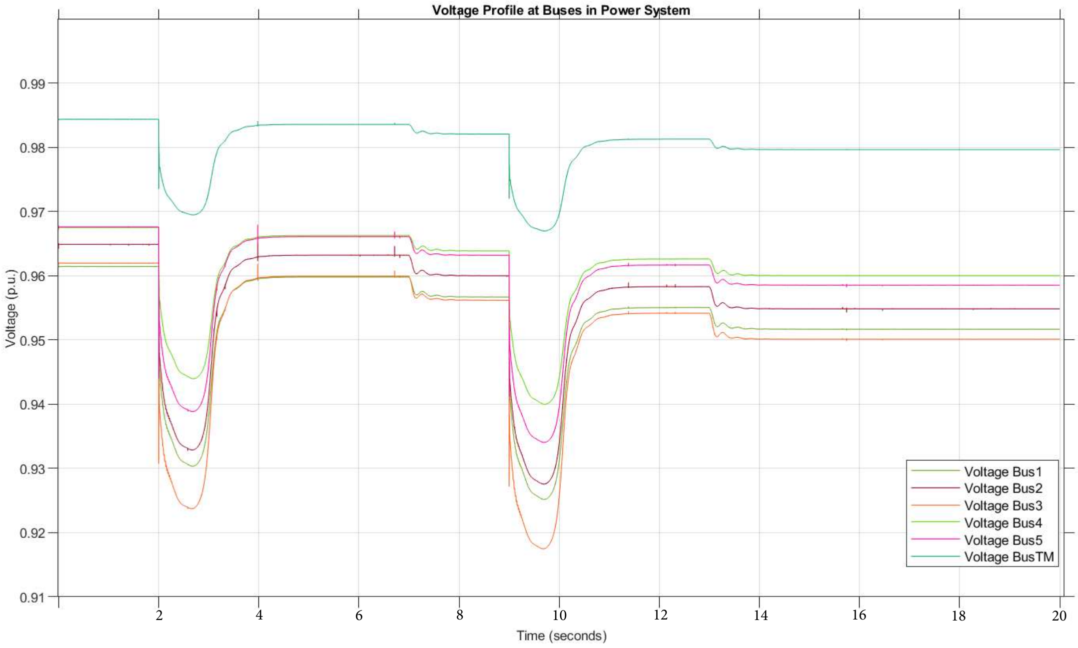

Figure 4.1: Voltage Sags originated during electric drill rigs oepration

As anticipated, Bus 3—being the most electrically distant and thus the most vulnerable—exhibits the most pronounced voltage deviations. Consequently, Bus 3 serves as the reference point for our comparative analysis, providing a clear benchmark against which the performance of alternative configurations, such as the Active Front End (AFE) scheme, will be evaluated. This methodical approach ensures that the impact of each configuration on system stability and voltage quality is thoroughly assessed.

4.1.1 Driller with DOl as starting method

As previously discussed, employing Direct-On-Line (DOL) starters as the motor control strategy induces significant voltage drops during the magnetization phase, primarily due to the high starting current demand. The severity of this phenomenon depends on the strength of the electrical grid. Stronger grids exhibit minimal voltage deviation, as they are better equipped to supply the large reactive power required during motor startup. On the other side, weaker grids experience more pronounced voltage depressions, which—under critical conditions—may trigger voltage collapse phenomena.

To assess the system's vulnerability under varying grid conditions, a parametric sweep of the grid strength was conducted. Grid strength was characterized by the Grid Strength Ratio (GSR), defined as:

$$\mathrm{GSR} = \frac{S_{\mathrm{SC,PCC}}}{S_{\mathrm{TX}}} \tag{4.1}$$

where $S_{\mathrm{SC,PCC}}$ denotes the three-phase short-circuit capacity at the point of common coupling (PCC), and S_{TX} represents the rated power of the main feeder transformer. The analysis progressively reduced $S_{\mathrm{SC,PCC}}$ from 400 MVA to 80 MVA, corresponding to a GSR range of $8.0 \rightarrow 1.6$. During this sweep, sequential energization of the two drill rig induction motors using DOL starters introduced two distinct voltage disturbance events into the network, allowing a quantitative evaluation of the severity of sag across the GSR range studied.

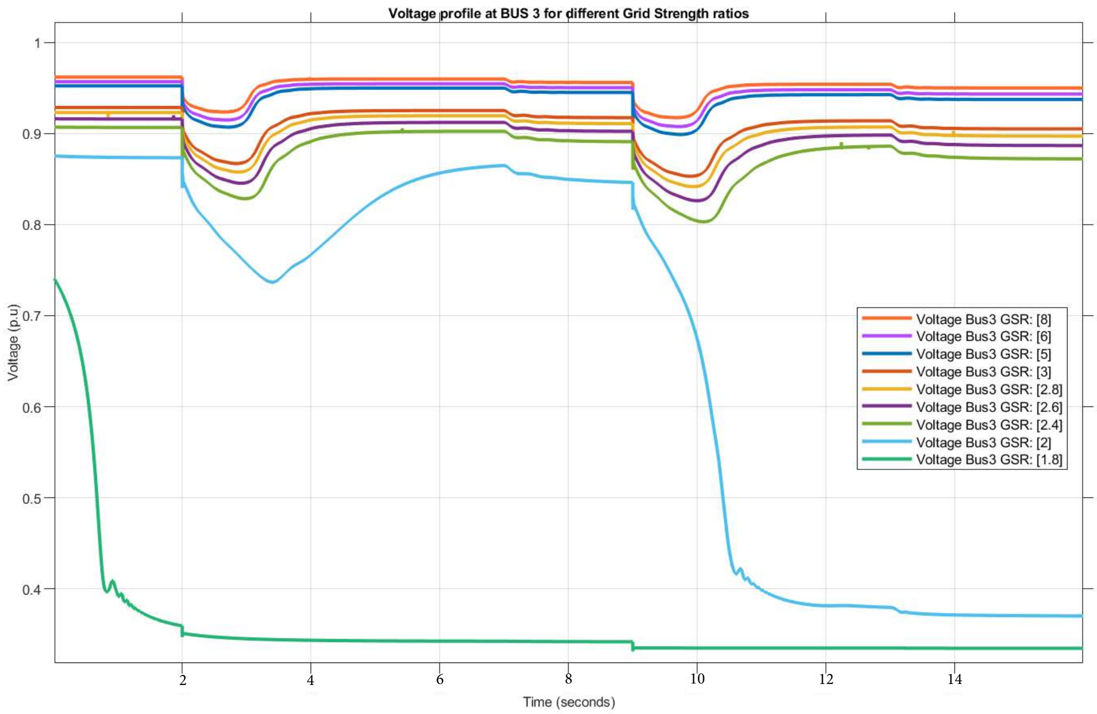

Figure 4.2: BUS 3 voltage profile for several grid strength ratios under DOL operation

In the continued development of the project, as shown in Figure 4.2 a series of simulation sweeps were conducted to characterize the voltage sag phenomenon expected during the drilling operation. Specifically, it was observed that each driller, under the current Direct-On-Line (DOL) connection, induces a voltage sag during its magnetization phase and a subsequent reduction in the voltage profile during peak load conditions due to the increased power demand.

For grid strength ratios (GSR) of 8, 6, and 5, no voltage sags were recorded according to the IEC61000-4-30 standard metrics [51]. However, each scenario did exhibit a noticeable depression in voltage relative to the pre-energization steady-state values. The critical threshold at which voltage sags began to manifest was identified at a GSR of 3, corresponding to a short-circuit capacity of 150 MVA. From this point down to the minimum tested GSR of 1.4, the voltage sags increased in both depth and duration.

At a GSR of 3, two distinct voltage sags were observed, each followed by a recovery once the magnetization phase concluded. However, at a GSR of 2.4, the post-recovery voltage settled at the lower acceptable limit, and although the system maintained stability without oscillations, the steady-state voltage remained at 0.87 p.u., outside the desired regulation range. According to IEEE and IEC standards, this represents a clear voltage sag, which could potentially be addressed in conjunction with system protection coordination strategies.

In the most severe scenario, with a GSR of 1.6 (80 MVA short-circuit capacity), the system failed to maintain stability during the magnetization of the first driller, resulting in a complete collapse of the voltage profile. This makes the data for GSR values of 3 and 2.4 particularly significant, as they will serve as the basis for a more in-depth comparison with the proposed Active Front End (AFE) solution.

Table 4.1: Voltage Sag and Reactive Power Demand — DOL_DOL Scenario

Item	**SCC [MVA]**	**GSR**	**Bus #**	**Sag 1 [p.u.]**	**Dur. 1 [s]**	**Sag 2 [p.u.]**	**Dur. 2 [s]**	**SS Final Voltage [p.u.]**	**Reactive Power in SS [MVAR]**
1	400	8	3	NO Vsag	NO Vsag	NO Vsag	NO Vsag	0.9501	0.7343
2	300	6	3	NO Vsag	NO Vsag	NO Vsag	NO Vsag	0.9430	0.9020
3	250	5	3	NO Vsag	NO Vsag	NO Vsag	NO Vsag	0.9370	0.9190
4	200	4	3	0.894	0.638	0.884	NO Vsag	0.9270	0.9500
5	150	3	3	0.867	1.237	0.853	1.6428	0.9051	3.0450
6	140	2.8	3	0.828	2.5684	0.803	12.9168	0.8970	1.0490
7	130	2.6	3	0.845	1.7478	0.826	3.5960	0.8870	1.0870
8	120	2.4	3	0.828	2.5684	0.803	12.9168	0.8720	7.2840
9	100	2	3	Unstable	Unstable	Unstable	Unstable	0.3700	2.0810
10	80	1.6	3	Unstable	Unstable	Unstable	Unstable	0.3340	1.0170

The data presented in Table 4.1 reveals three clearly defined operating regimes that are depending on the available short-circuit capacity (SCC) and the resulting grid strength. When the SCC is at least 250 MVA (Grid Strength ≥ 5), direct-on-line motor start sequence cause no perceptible voltage sag and the post-start voltage remains around 0.94–0.95 p.u.; reactive-power demand stays modest at roughly 0.73–0.92 MVAr, showing that a stiff network can absorb inrush current without affecting the voltage profile. As the SCC falls into the 200–120 MVA band (Grid 4–2.4), deep sags start to present in the system: the first dip can reach 0.828 p.u. and stretch from 0.6 s to more than 2.5 s, while a second dip may linger for up to 13 s. In conclusion, reactive-power demand rises non-linearly, peaking between 3.0 and 7.3 MVAr—evidence that synchronous machines and compensation banks are straining to hold the voltage up.

Operationally, these findings mean that simultaneous DOL starts should be limited to networks with SCC $\geq$ 250 MVA unless additional countermeasures are in place. Within the 200–150 MVA range, installing dynamic var support such as an SVC or STATCOM rated for at least 7 MVAr and fine-tuning protection settings to ride through sags down to 0.83 p.u. for three seconds is advisable. Its worth mentioning this suggestion was not fully explored in this thesis development but vaguely simulated as a comparison metric.

If grid strength is expected to dip below 150 MVA, migrating to soft-starters (not explored in this work) or variable-frequency drives that trim inrush to about 350–400% of full-load current helps avoid slipping into the unstable region. Finally, at SCC levels of 100 MVA or less, direct-on-line starts should be banned—or the grid reinforced—because the risk of voltage collapse and nuisance trips becomes unacceptably high.

4.2 Electric Driller with AFE under Unity PF control mode

In the scenario where the grid strength ratio is reduced to 2, corresponding to a short-circuit capacity of 100 MVA, the results, as illustrated in Figure 4.3, indicate that the bus voltage profile remains below the stipulated standard. However, despite not reaching the ideal voltage levels, the system maintains a stable voltage without experiencing a collapse. While this may not be the most optimal operational condition, it does indicate that the integration of the Active Front End (AFE) technology successfully extends the operational range of the system.

In comparison to the DOL scenario, where the operational limit was constrained to a grid strength ratio of around 2.4, the incorporation of the AFE allows for stable operation even at a ratio of 2. This enhancement indicates a significant improvement in the system's robustness and flexibility, enabling it to operate under weaker grid conditions without compromising stability.

However, at even lower grid strengths, such as a ratio of 1.6, a total voltage collapse is observed. This collapse is influenced by external demands from other machinery not utilizing the AFE technology, highlighting the importance of comprehensive system-wide implementation for optimal performance.

Figure 4.3: BUS 3 voltage profile for several grid strength ratios

Table 4.2: Steady-State Voltage and Reactive Power Demand Comparison for both drillers using DOL starting mechanism and both drillers using AFE

Item	SCC [MVA]	Grid Strength	DOL_DOL		AFE_AFE	
			V [p.u.]	Q [MVAr]	V [p.u.]	Q [MVAr]
1	150	3.0	0.9051	3.0450	0.9180	0.5260
2	140	2.8	0.8970	1.0490	0.9120	0.5377
3	130	2.6	0.8870	1.0870	0.9038	0.5550
4	120	2.4	0.8720	7.2840	0.8922	0.5716
5	100	2.0	0.3700	2.0810	0.8410	0.6650
6	80	1.6	0.3340	1.0170	0.3390	1.5500

When comparing the performance of the DOL and AFE configurations under weaker grid conditions, it becomes evident that the integration of the Active Front End significantly enhances system stability and performance. In scenarios where the grid strength ratio decreases, the AFE configuration demonstrates a clear advantage by preventing voltage sags that would otherwise be present in the DOL setup.

Notably, as the short-circuit capacity decreases, the AFE configuration maintains a more consistent and stable voltage profile. While the DOL system starts to show significant voltage instability at a grid strength ratio of 3 (150 MVA), the AFE system only begins to face challenges at a ratio of 2.4 (120 MVA), thereby extending the operational threshold and ensuring more robust performance.

In terms of reactive power demand, the AFE configuration keeps this demand relatively stable, with variations in the kilovolt-ampere reactive range, as opposed to the megavolt-ampere reactive variations seen in the DOL configuration. Ultimately, even if a voltage collapse occurs at extremely low grid strengths (such as a ratio of 1.6 or 80 MVA), this collapse is attributed to external factors beyond the control of the AFE-equipped drillers.

In conclusion, the implementation of AFE technology allows for extended and stable operation under weaker grid conditions, making it possible for the equipment to adapt to less ideal networks without causing additional stress on the existing infrastructure.

4.3 AFE Driller with compensation capability

The advantages of using the AFE drive as the connection method compared to classical DOL were demonstrated in a previous section. Although the voltage profile is improved because the reactive power demand at machine start is reduced, implementing AFE drives in all drilling units is very expensive. As a result, another scenario was evaluated, in which a drilling unit using the AFE method of connection was modified to include reactive power compensation capability. This modification in the control of the AFE rectifier is shown in Figure 3.3. The machines involved in the scenario are highlighted in Figure 4.4.

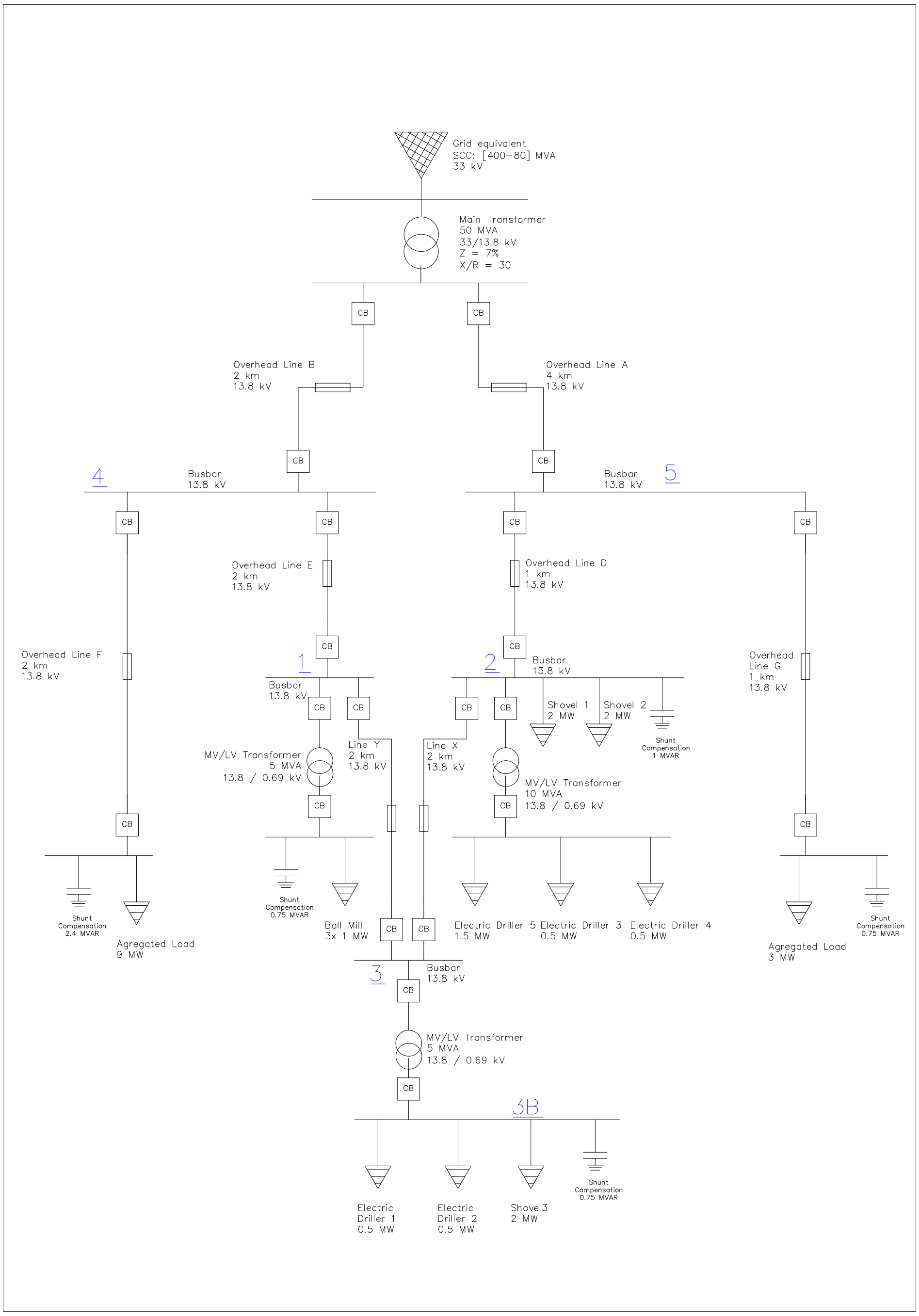

Figure 4.4: Single line diagram of test grid with machines used in scenario 3

Aggregated loads at buses 4 and 5, the ball mill at bus 1, and shovels at buses 2 and 3 utilize fixed compensation through capacitor banks. In contrast, drilling unit 1 employs the reactive compensation capability of the AFE rectifier, while drilling unit 2 operates without compensation. Table **??** presents the characteristics of these machines.

4.3.1 Minimum Grid Strength

An analysis of grid strength variations, similar to that done in Scenario 1, was performed for Scenario 3. The parametric sweep started at 5 and ended at 2.4. The grid strength was decreased by 1 until it reaches a value of 3. Then, from grid strength 3, it was decreased in smaller intervals of 0.2. This was done with the objective of finding the critical grid strength threshold at which the system maintains operation within acceptable limits. The results are displayed in Figure 4.5.

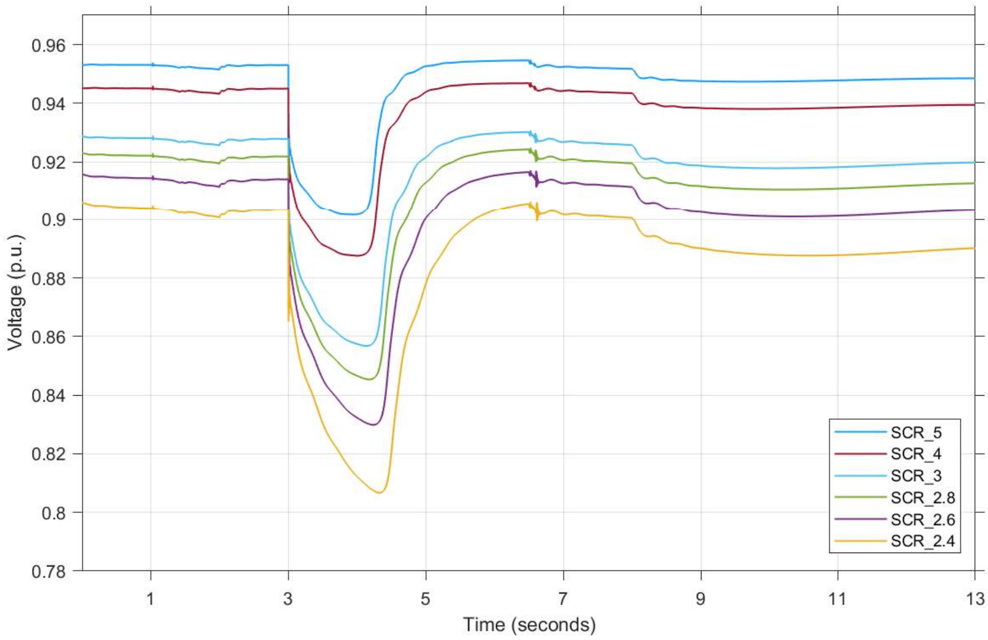

Figure 4.5: Bus 3 voltage profile for several grid strength ratios in scenario 3 conditions

As expected, when the short circuit ratio of the grid is reduced, the system is more sensitive to disturbances and requires more time to recover from them. This behavior is clearly demonstrated in the two boundary condition plots. At a grid strength of 5.0, the magnetization transient of drilling unit 2 has minimal impact on the voltage profile at bus 3, with voltage levels remaining within acceptable operational limits. In contrast, when the grid strength is reduced to 2.4, the magnetization of the same unit generates a voltage sag of approximately 10% below previous voltage level, with a duration of nearly 3 seconds.

When comparing the results between scenario 1 and scenario 3, it is clear that the impact of the reactive compensation given by the driller unit with AFE drive modified is positive. In Table 4.3 are shown results for three different grid strengths. As the short circuit capacity is decreased in the system, the sag duration is reduced when AFE drive is used in the drilling unit. As a result, the grid can recover from the start-up of the induction motor faster, preventing the triggering of protective devices.

Additionally, the voltage profile presents consistently higher value in scenario 3 compared to scenario 1. This can reduce the fixed reactive compensation that the grid would be needed, as it allows simultaneous operation of driller units that later can move to a different area in the pit.

Table 4.3: Comparison of Voltage sag at bus 3 between Scenarios 1 and 3

Grid Strength	**Scenario 1**		**Scenario 3**	
	Sag	**Duration**	**Sag**	**Duration**
3	0.853 pu	1.62 s	0.857 pu	1.5 s
2.8	0.0.842 pu	2 s	0.845 pu	1.71 s
2.6	0.826 pu	4 s	0.830 pu	2 s

Results for different grid strength are displayed on Table 4.4. As discussed in previous section, the last stable configuration for the grid when drilling units implement DOL method of connection is 2.8. The improvement in voltage level in scenario 3 respect scenario 1 is about 1.5 %. When driller units implement the AFE drive as method of connection, the grid strength can be decreased more and the voltage profile in steady state remain within acceptable limits. When comparing scenario 2 and scenario 3, the difference in voltage profile in steady state are minimal. However, in scenario 3 only one drilling unit implements AFE drive modified. As a result, the reactive power compensation capability allow to operate a drilling unit with classical method of connection, having the same voltage profiles in steady state as in scenario 2.

Table 4.4: Comparison of steady state voltage at bus 3

Grid Strength	**Steady state voltage profile**		
	Scenario 1	**Scenario 2**	**Scenario 3**
3	0.905 pu	0.917 pu	0.919 pu
2.8	0.897 pu	0.911 pu	0.912 pu
2.6	0.8868 pu	0.9025 pu	0.9020 pu

Upon analysis, the active power drawn from the grid by the AFE converter is directly transferred to the motor, as illustrated in Figure 4.6. This characteristic results from the power factor correction implemented within the converter control system. This functionality improves motor efficiency and reduces system losses. Additionally, when the power factor approaches unity, the reactive power consumption is minimized, and hence the voltage profile at the bus presents better levels than compared with Scenario 1.

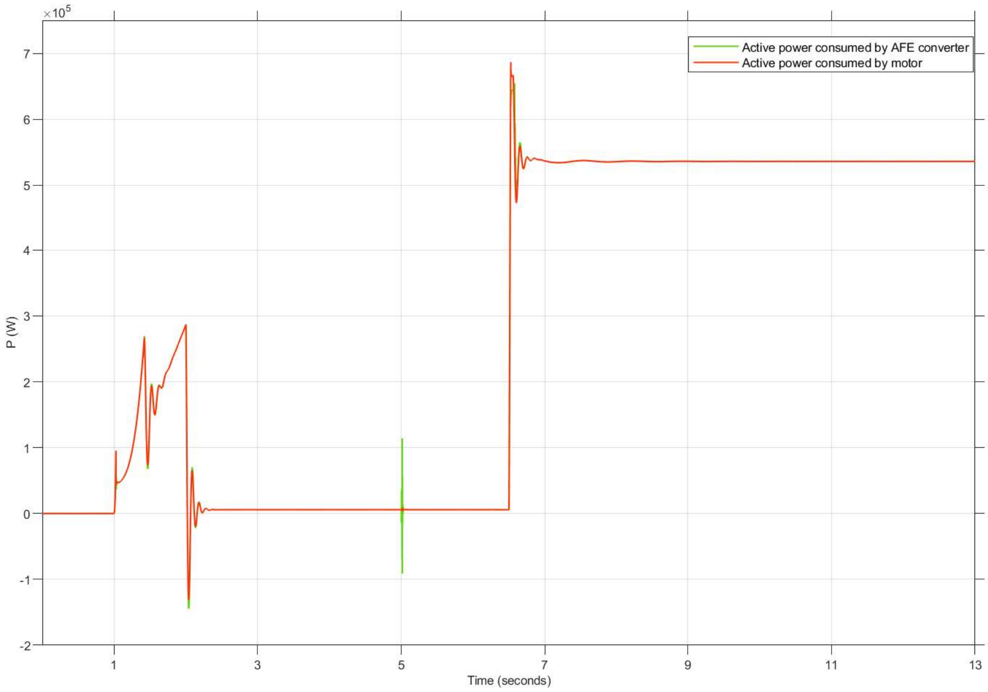

Figure 4.6: Active power consumed by the motor vs AFE drive

On the other hand, when the focus is on reactive power, Figure 4.7 presents the consumption of AFE converter and motor. When induction motor is magnetized at second 1, the reactive power required is provided by the AFE converter. At second 3, the reactive compensation is enabled, and it starts to inject reactive current to the grid. This is due the threshold to activate the compensation was triggered. From second 3 to 5, the AFE converter continues providing reactive support. At second 5, the second drilling unit started magnetization, causing the reactive compensation to increased. Finally, driller unit 1 went to full load operation just before second 7. As a result, there is a peak in the reactive power consumed by the motor and simultaneously, the reactive compensation is increased to mitigate this rose in the reactive power consumption at the bus.

Throughout the simulation period, the reactive power consumed by the motor was supplied by the AFE drive. Moreover, once the AFE drive starts to provide reactive power compensation to the bus, when the driller starts operation with a full load, the compensation was increased to cover the reactive power consumed by the motor. As the reactive power consumed by all the driller units is partially supplied by the AFE converter, this allows the bus voltage to maintain a profile above 0.9 per unit. As a result, the voltage profile is similar to Scenario 2 with the difference that only one driller unit is equipped with an AFE drive.

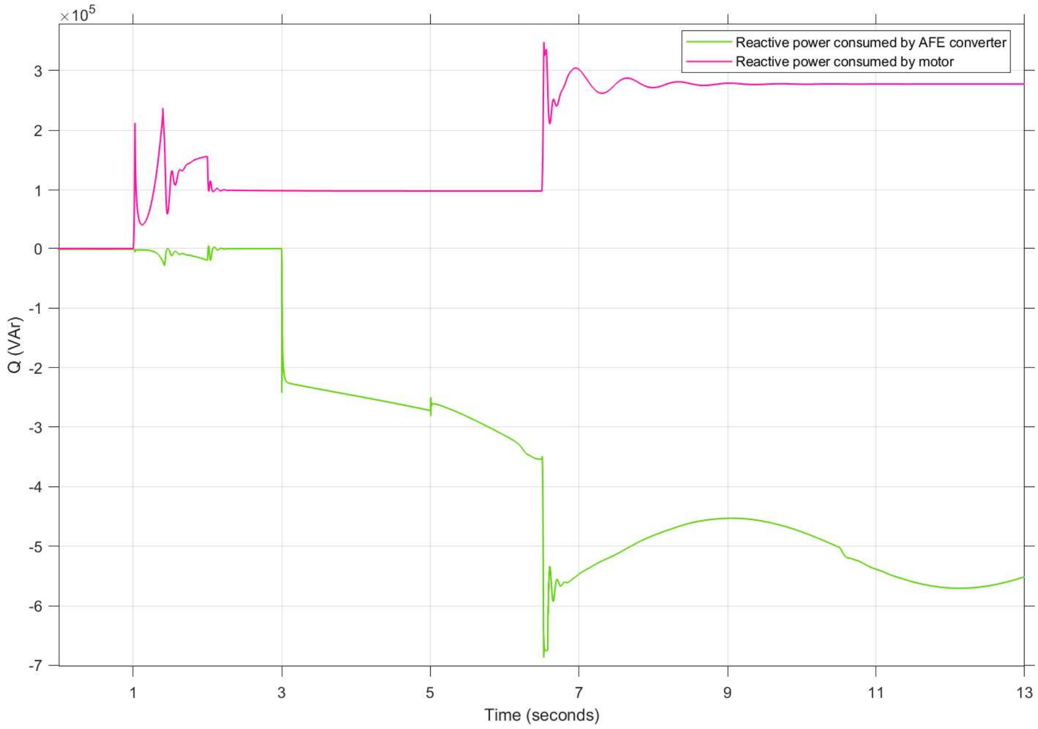

Figure 4.7: Reactive power consumed by the motor vs AFE drive

4.3.2 Maximum operational driller units

Once the minimum grid strength in which the mine grid has stable operation was found, the next question to solve was the maximum number of drilling units that the mine grid can operate without compromising stability while utilizing the reactive compensation capability of the AFE drive. It was found that three drilling units can be operated under a grid strength of 2.8. In Figure 4.8 is shown the voltage profile of bus 3 when the short circuit capacity is 140 MVA. The voltage level is similar to the voltage level when 2 driller operate at full load condition under grid strength of 2.6.

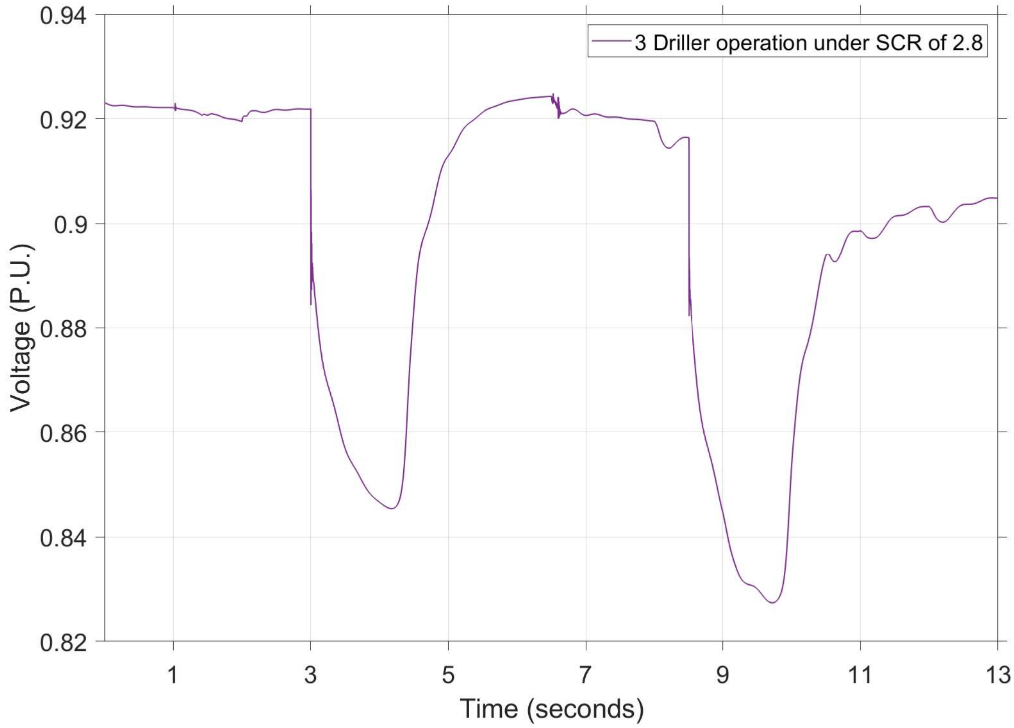

Figure 4.8: Bus 3 voltage profile with 3 drilling units operating

The analysis revealed that reactive compensation alone is insufficient to enable the operation of a third drilling unit under a grid strength of 2.6. However, when the grid strength is increased to 2.8, a third drilling unit can operate successfully while maintaining voltage profiles within acceptable limits. This represents a 50% increase in drilling production capacity compared to Scenario 1 and Scenario 2.

From this analysis, it is clear that the reactive power compensation provided by the AFE converter significantly enhances the voltage stability of the electrical grid. This compensation capability enables the operation of drilling units utilizing DOL connection methods under weaker grid conditions that would otherwise be unsuitable. Furthermore, the system effectively reduces both the magnitude and duration of voltage sags when additional drilling units cause transients due to magnetization. The steady-state voltage profiles achieved through this compensation approach are comparable to those observed in Scenario 2, where both drilling units are equipped with AFE converters, demonstrating equivalent performance benefits at reduced implementation costs.

4.4 Discussion

In Figure 4.9 two disturbance windows (≈2–4 s and ≈ 9–12 s, dashed magenta boxes) are highlighted and the contrast between DOL and AFE is unambiguous. Under DOL, the traces are 'stacked' by grid strength: As the GSR decreases from 3.0 to 2.0, the first event deepens from a mild dip to roughly 0.73 p.u. and the second event becomes markedly worse. At GSR = 2.0 the second event triggers a dynamic collapse: the bus voltage plunges below 0.40 p.u. and does not recover, consistent with the unstable regime identified in the table. This monotonic ordering with GSR is typical of inrush-driven sags in weak systems: a higher Thevenin impedance yields larger voltage drops and longer settling.

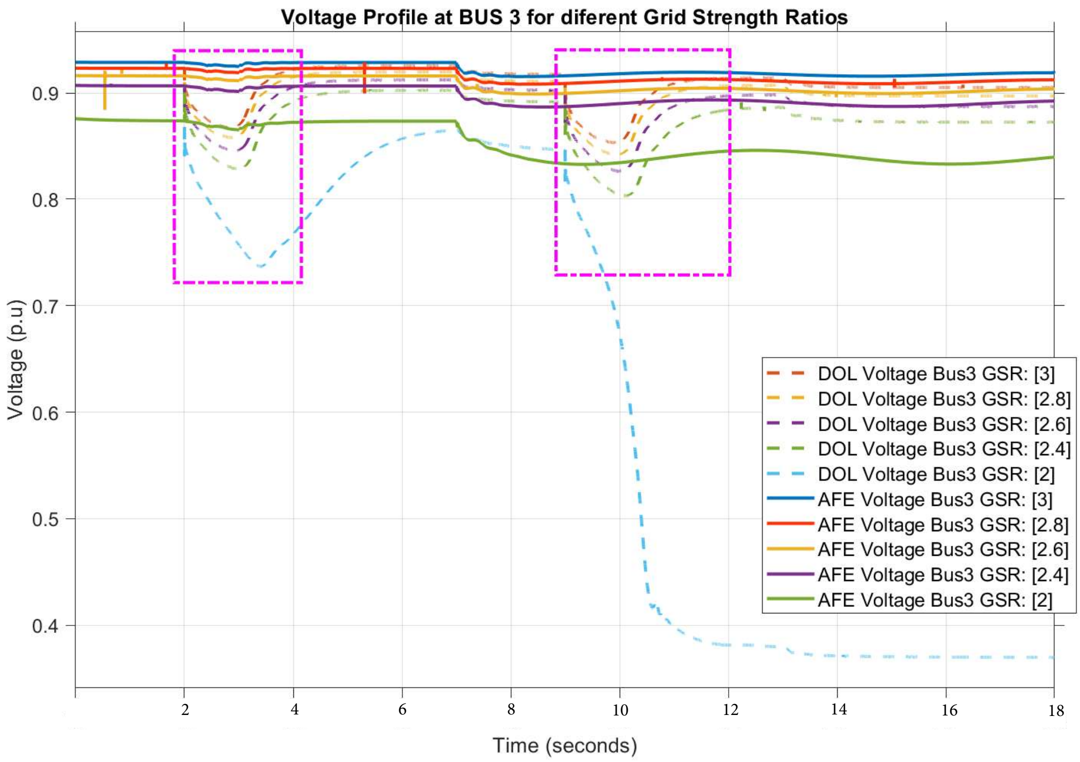

Figure 4.9: BUS 3 voltage profile for several grid strength ratios

In contrast, the AFE curves remain tightly clustered across all GSR values, with the bus voltage held around 0.90–0.93 p.u. during both events and returning smoothly to its pre-disturbance level. The absence of progressive deepening from the first to the second event indicates that the AFE effectively decouples the motor starting current from the upstream grid, limiting transient reactive demand and preventing compounding sags. The only visible defect is a small steady-state ripple once the events end; this can be attributed to the inner-loop controller tuning. Its amplitude is minor, well within typical steady-state voltage-quality range, and does not threaten operational margins.

Taken together, the figure shows that AFE control extends the stable operating envelope by at least one full GSR step relative to DOL (i.e., what collapses under DOL at GSR ≈ 2 remains stable with AFE). Even operated at unity power factor, the AFE removes the second-event comparing to DOL and maintains acceptable voltages levels. This directly supports the earlier quantitative findings: DOL becomes increasingly sensitive to grid weakness and multi-event sequences, whereas

AFE keeps the bus voltage largely insensitive to upstream short-circuit capacity over the tested range.

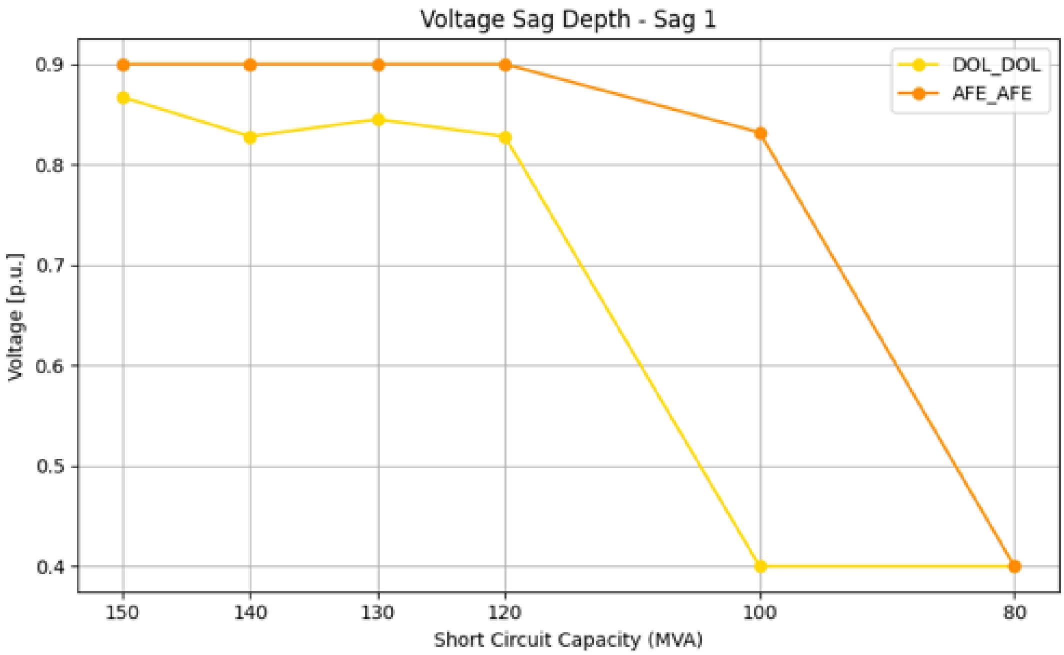

(a) Vsag1 comparisson betwen DOL and AFE

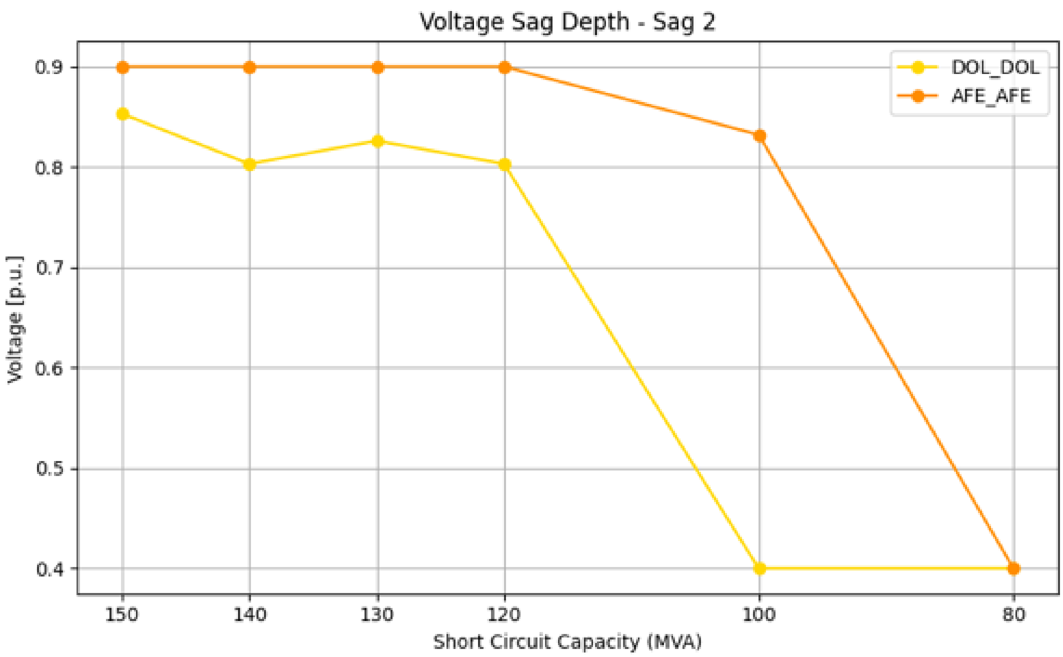

(b) Vsag2 comparisson betwen DOL and AFE

Figure 4.10: Sags deepness comparisson betwen DOL and AFE

Across the evaluated short-circuit ratio (SCR) band of 3 SCR 2, the conventional

Direct-On-Line (DOL) starting method exhibits a continuous deterioration in voltage-sag severity. Successive disturbance events compound this effect: during Event 2—initiated on an already weakened grid, the retained voltage reaches a markedly lower minimum than in Event 1, confirming that DOL-driven motors impose progressively deeper sags as grid impedance rises.

By contrast, drillers equipped with an Active Front End (AFE) converter maintain a substantially flatter voltage profile over the same SCR range. Both events demonstrate that the AFE mitigates inrush currents and regulates reactive power exchange, thereby suppressing the development of significant voltage sags. Even under the compounded loading of Event 2, the bus voltage remains within a stable, non-collapsing voltage, enabling parallel operation with other large drives without imposing severe disturbances to the system stability.

Consequently, the AFE topology extends the permissible operating boundary of the installation from the DOL limit of approximately SCR $\approx$ 2.4 down to SCR $\approx$ 2.0 while preserving voltage stability. This improvement not only reduces the risk of under-voltage trips and ancillary equipment maloperation but also provides additional headroom for future load integration on the same electrical infrastructure, converting the AFE implementation into a strategic enhancement rather than a mere control-scheme substitution.

4.5 Ethics

Throughout this project, particular attention has been given to ensuring transparency and honesty in how the study was conducted and how its results are presented. Since detailed manufacturer data for the electric machines were not available, the motor parameters used in the simulations were derived from theoretical estimations and representative values found in the literature. This approach allowed the work to move forward without compromising the quality of the analysis, while being clear that the numerical results reflect realistic trends rather than the exact behavior of a specific industrial machine.

It is ethically important to recognize the limitations that come with this choice. Without experimental validation, certain aspects of the model; especially those related to transient behavior and losses; remain uncertain. A complete characterization of the actual motors, including locked-rotor and no-load tests, would be necessary in future work to obtain precise equivalent circuit parameters. Such tests would strengthen the reliability of the findings and help bridge the gap between theoretical modeling and real operational performance.

Finally, the ethical responsibility of this work extends to communicating its purpose clearly. The models, results, and conclusions are not intended to serve as definitive design recommendations, but as a contribution to the broader understanding of grid-connected electric machinery and voltage stability in open-pit mining networks. Acknowledging assumptions, uncertainties, and future needs ensures that the research remains credible, transparent, and aligned with good engineering practice.

Artificial intelligence tools were employed exclusively to assist in text validation, translation, LaTeX formatting, and numerical result analysis. The entirety of the technical content, methodology, and interpretations presented in this thesis are fully original and developed by the student authors.

4.6 Sustainability

This project has been developed with a clear awareness of its potential contribution to a more sustainable mining industry. Open-pit mines are traditionally associated with high energy consumption and significant greenhouse gas emissions, largely due to the reliance on diesel-powered equipment. By exploring the integration of electrically driven blasthole drillers and Active Front-End (AFE) converters, this work supports the broader transition toward cleaner and more efficient mining operations. Electrification not only reduces direct emissions but also opens the door to using renewable energy sources within the mine's electrical network.

Beyond its environmental implications, sustainability in this context also involves improving the efficiency and reliability of electrical systems. The proposed converter-based configurations and control strategies aim to reduce voltage disturbances, optimize power quality, and minimize reactive power demand. These improvements, although technical in nature, have tangible long-term benefits: they can lower operational energy losses, reduce wear on equipment, and extend the lifespan of electrical assets. Over time, these factors contribute to both economic and environmental sustainability by promoting more responsible use of energy and infrastructure.

While the scope of this thesis is primarily analytical and simulation-based, its outcomes provide valuable insights for designing the next generation of sustainable mining systems. The results highlight that technological innovation and environmental responsibility can go hand in hand when efficiency, stability, and emission reduction are treated as interconnected goals. In that sense, this research not only addresses an engineering challenge but also contributes to the collective effort of decarbonizing one of the world's most energy-intensive industries.

5

Conclusions and Future Work

5.1 Conclusions

This thesis presented a comprehensive evaluation of the connection between two strategies for high-power drilling units in open-pit mining with a particular focus on voltage stability and voltage sag mitigation. A detailed grid model was developed to replicate typical mining load characteristics and parametric sweeps across short-circuit ratios (2.4–5.0) were performed to identify the most critical scenarios where the machines could theoretically operate without risking stability problems. Three alternatives were studied: conventional Direct-On-Line (DOL) connection, full Active Front End (AFE) drive deployment, and a hybrid configuration based on selective AFE implementation with reactive power compensation.

The analysis confirmed that AFE technology provides the strongest technical performance under weak-grid conditions. It improves steady-state voltage profiles, reduces grid stress, and enhances motor dynamics. However, full deployment across all units is limited by cost and complexity. To address this, the study developed and tested a modified control strategy for AFE rectifiers that enables them to deliver reactive power support. This hybrid solution demonstrated the ability to achieve near-equivalent performance to full AFE deployment, while requiring a lower investment.

The principal findings and conclusions are detailed below:

- **Performance of AFE drives**
  - Superior steady-state voltage support under weak-grid conditions compared to Direct on Line.
  - Capability to inject reactive current, improving power factor and reducing grid losses and strict dependancy on the SCR of the PCC to satisfy the needs of the mine power system.
  - Flux-oriented control enhanced low-speed torque, enabling smoother acceleration.
  - Reduction of torque oscillations, lowering mechanical stress during start-up.
- **Hybrid approach with reactive compensation**
  - Enabled stable operation under minimum SCR of 2.6, where DOL was no longer feasible.
  - Maintained bus voltage levels above 0.9 p.u. even under critical grid strengths.

  - Limited by converter maximum current capacity, but still provided substantial reactive support.
  - Voltage sag depth and duration were reduced, with weak grids showing steady-state voltages up to 1.5% higher than Direct on Line.
- **Impact on production capacity**
  - Reactive compensation allowed up to 50% increase in drilling production under specific weak-grid scenarios.
  - Reduced downtime associated with deep and long voltage sags.
  - Provided more stable operation during sequential starts of large mining equipment.
  - As voltage sag duration as deepness was reduced, chances to experience under voltage protection triggering are mitigated.
- **Economic and operational considerations**
  - Full AFE deployment provides maximum benefits but requires high capital investment.
  - Hybrid AFE deployment achieves comparable voltage stability improvements at lower cost.
  - Selective approach shortens return-on-investment time by avoiding full fleet conversion.
  - Hybrid configuration allows a modular solution *"plug&play"* approach for using electric drillers in weak grid scenarios.
- **Overall system impact**
  - Voltage disturbances caused by drilling unit magnetization can be effectively mitigated through AFE-based compensation.
  - The hybrid control modification reproduces steady-state profiles similar to full AFE while reducing system costs.
  - Strategic AFE deployment strengthens weak mining grids, increases production capacity, and improves long-term system reliability.

In conclusion, the results establish that selective AFE implementation with reactive compensation represents a technically sound and economically viable solution for mining operations. The approach balances cost and performance, demonstrating that hybrid AFE deployment can provide stable voltage profiles, enhance production, and ensure robust operation under challenging grid conditions.

5.2 Future Work

After developing this thesis project, the following future work areas were identified.

Advanced control strategies for the AFE should be investigated beyond the present grid-following unity-power-factor mode. A first step is to implement a grid-forming option, removing the PLL and adding voltage/frequency droop—to test whether the stable operating condition can be extended in very weak grids (GSR $\leq$ 2). In grid-following mode, an adaptive Volt/Var hierarchy is recommended: an outer bus-voltage regulator that generates i_q^* with explicit current limits, anti-windup, and rate limiters, and inner current loops tuned for adequate phase-margin under wide impedance variation.

At the mine-system level, coordinated Volt/Var control across multiple assets (electric rig drillers) should be developed to avoid over-compensation. A practical architecture is a leader–follower scheme where one AFE (or an existing STATCOM/SVC) sets a bus-voltage reference and secondary devices share reactive current via droop characteristics. Also start-up sequencing of drillers and shovels should be optimized to minimize overlap of inrush events while respecting production constraints, comparing scheduled versus free operation. An optimization study for the number, rating, and placement of AFEs can be explored in order to meet voltage KPIs with minimum CAPEX.

Finally, integration with energy storage and on-site renewables should be explored to complement reactive support. A DC-coupled BESS sharing the AFE DC link can inject active power during transients to arrest voltage decay, while the AFE provides fast Q; their coordination can be implemented with a a controller using MPC that allocates P and Q based on predicted events and state-of-charge. This line of study can help quantify the incremental benefit of $P + Q$ support versus Q-only in terms of sag depth reduction, recovery time, and avoided trips.

Bibliography

[1] N. Ertugrul, ”Mine Electrification and Power Electronics: The roles of wide-bandgap devices,” *IEEE Electrification Magazine*, vol. 12, no. 1, pp. 6–15, 2024.

[2] F. Sánchez and P. Hartlieb, ”Innovation in the mining industry: Technological trends and a case study of the challenges of disruptive innovation,” *Mining, Metallurgy & Exploration*, vol. 37, no. 5, pp. 1385–1399, 2020.

[3] N. Maennling and P. Toledano, ”The renewable power of the mine,” *Available at SSRN 3661616*, 2018.

[4] Epiroc Group, ”About the Epiroc Group,” *Available at Epiroc Group*, 2025.

[5] H. L. Hartman and J. M. Mutmansky, *Introductory Mining Engineering*. John Wiley & Sons, 2002.

[6] J. Chadwick, *Mining Explained: A Layman's Guide*. Elsevier, 2011.

[7] L. Morán, J. Espinoza, and R. Burgos, "Voltage regulation in mine power distribution systems: Problems and solutions," in *2014 IEEE Industry Application Society Annual Meeting*, 2014, pp. 1-7. doi: 10.1109/IAS.2014.6978453.

[8] J. Yaghoobi, A. Abdullah, D. Kumar, F. Zare, and H. Soltani, "Power Quality Issues of Distorted and Weak Distribution Networks in Mining Industry: A Review," *IEEE Access*, vol. 7, pp. 162500-162518, 2019. doi: 10.1109/ACCESS.2019.2950911.

[9] N. Ertugrul, A. P. Kani, M. Davies, D. Sbarbaro, and L. Morán, "Status of Mine Electrification and Future Potentials," in *2020 International Conference on Smart Grids and Energy Systems (SGES)*, 2020, pp. 151-156. doi: 10.1109/SGES51519.2020.00034.

[10] L. Morán, J. Espinoza, and R. Burgos, "Voltage regulation in mine power distribution systems: Problems and solutions," in *2014 IEEE Industry Application Society Annual Meeting*, 2014, pp. 1-7. doi: 10.1109/IAS.2014.6978453.

[11] J. Yaghoobi, A. Abdullah, D. Kumar, F. Zare, and H. Soltani, "Power Quality Issues of Distorted and Weak Distribution Networks in Mining Industry: A Review," *IEEE Access*, vol. 7, pp. 162500-162518, 2019. doi: 10.1109/

[12] H. Jeronen, T. West, J. Kerttula, T. Humalamaa, J.-M. Lupin, and E. Delaunay, "Mining Power System: Recommended Power Generation and Electrical Distribution for High Altitude Lithium Mine," Wärtsilä White Paper, June 2021. [Online]. Available: `https://www.wartsila.com/docs/default-source/power-plants-documents/downloads/white-papers/w%C3%A4rtsil%C3%A4-energy---business-white-paper---mining-power-system.pdf`

[13] IEEE Power & Energy Society, “Definition and Classification of Power System Stability,” *IEEE Transactions on Power Systems*, vol. 19, no. 2, pp. 1387–1401, 2004. DOI: 10.1109/TPWRS.2004.825981.

[14] T. Van Cutsem, “Voltage instability: Phenomena, countermeasures, and analysis methods,” *IEEE Transactions on Power Systems*, vol. 15, no. 3, pp. 593–601, Aug. 2000.

[15] Y. Wang, C. Li, L. Zhang, Z. Xu, H. Sun, and Y. Xu, “Voltage stability assessment of power systems: Methods, challenges and future trends,” *Journal of Modern Power Systems and Clean Energy*, vol. 11, no. 11, pp. 1481–1499, Nov. 2023. [Online]. Available: `https://www.sciencedirect.com/science/article/pii/S2213138823005313`

[16] N. Hatziargyriou *et al.*, “Stability Definitions and Characterization in Systems with High Penetration of Power Electronics,” *CIGRE Science & Engineering*, vol. 14, pp. 6–14, 2019.

[17] E. V. Stangler, F. A. S. Neves, F. J. Zimann, and M. Mezaroba, “Coordinated Control of Active and Reactive Power Compensation for Voltage Regulation with Enhanced Disturbance Rejection Using Repetitive Vector-Control,” *ResearchGate*, 2020. Available: https://www.researchgate.net/publication/341848795

[18] Dougherty, H. N., & Schissler, A. P. (2020). *SME mining reference handbook*. Society for Mining, Metallurgy & Exploration.

[19] Hannah Ritchie, "Cars, planes, trains: where do CO2 emissions from transport come from?", *Our World in Data*, 2020. `https://ourworldindata.org/co2-emissions-from-transport`.

[20] Luis Morán, Daniel Sbarbaro, Franco Ortega, and José Espinoza, *Electrical energy consumption characterization of open-pit mining and mineral processing operations towards the use of renewable energy sources*, 2019 IEEE Industry Applications Society Annual Meeting, pp. 1–6, 2019.

[21] Juan S. Gómez, Jose Rodriguez, Cristian Garcia, Luca Tarisciotti, Freddy Flores-Bahamonde, Javier Pereda, Felipe Nuñez, Aldo Z. Cipriano, and Juan Carlos Salas, *An overview of microgrids challenges in the mining industry*, *IEEE Access*, vol. 8, pp. 191378–191393, 2020.

[22] José Rodríguez, Luis Morán, Jorge Pontt, José Espinoza, Rodrigo Díaz, and Eduardo Silva, *Operating experience of shovel drives for mining applications*, *IEEE Transactions on Industry Applications*, vol. 40, no. 2, pp. 664–671, 2004.

[23] MathWorks, *Three-Phase Asynchronous Drive with Sensorless Control.* Disponible en: `https://se.mathworks.com/help/sps/ug/three-phase-asynchronous-drive-with-sensorless-control.html` [Accedido: 20-jul-2025].

[24] R. Arias, J. Ramírez, H. González, and J. Vázquez, “Indirect vector control of an induction motor using space vector modulation technique,” *IOP Conference Series: Materials Science and Engineering*, vol. 1105, no. 1, p. 012006, 2021. Disponible en: `https://iopscience.iop.org/article/10.1088/1757-899X/1105/1/012006/pdf` [Accedido: 20-jul-2025].

[25] V. Gopal B. T., M. R. Shashi Kumar, and M. Umapathy, “A Comparative Performance Analysis of Indirect Vector Controlled Induction Motor Drive Using

Optimized AI Techniques," *International Journal of Engineering and Advanced Technology (IJEAT)*, vol. 9, no. 3, pp. 2249–8958, Feb. 2020. Disponible en: https://www.researchgate.net/publication/339475475 [Accedido: 20-jul-2025].

[26] U.S. Department of Energy, "Improving Motor and Drive System Performance: A Sourcebook for Industry," Advanced Manufacturing Office, 2nd ed., 2014. Disponible en: https://www1.eere.energy.gov/manufacturing/tech_assistance/pdfs/motor.pdf [Accedido: 20-jul-2025].

[27] MENZEL Elektromotoren GmbH, *MEBKSL / MEBKS / MEBKSW Modular Motor Series Catalog*, Berlin, Germany, 2021. Available: https://www.menzel-motors.com/fileadmin/user_upload/Downloads/Motorkataloge/Menzel_Katalog_Modulare_MEBKSL_MEBKS_MEBKSW_01.pdf

[28] A. Hughes and B. Drury, *Electric Motors and Drives: Fundamentals, Types and Applications*, Newnes, 2019.

[29] E. F. Figueiredo, "Rotating Electrical Machines," in *Springer Handbook of Power Systems*, K. O. Papailiou, Ed., Singapore: Springer Singapore, 2021, pp. 367–441. doi: 10.1007/978-981-32-9938-2_6. Available: https://doi.org/10.1007/978-981-32-9938-2_6

[30] R. Krishnan, *Electric Motor Drives: Modeling, Analysis, and Control*, Prentice Hall, 2001.

[31] M. Nambiar y Z. Konstantinovic, "Synchronous condensers in mining projects: Improving power system stability and short-circuit power," Mining Engineering, vol. 67, no. 1, pp. 38–44, ene. 2015. Reimpreso de ABB Switzerland. Paper no. TP-13-060 (primera sumisión nov. 2013). [Online]. Disponible: ABB technical brochure :contentReference[oaicite:1]index=1

[32] T. Kalitjuka, *Control of Voltage Source Converters for Power System Applications*, Master's thesis, Institutt for Elkraftteknikk, 2011.

[33] ENTSO-E, "Voltage Source Converters (VSC)," ENTSO-E Technopedia, [Online]. Available: https://www.entsoe.eu/technopedia/techsheets/voltage-source-converters-vsc/. [Accessed: 23-Jul-2025].

[34] D. Lundin, *Control of Voltage Source Converter in HVDC*, Master's thesis, Uppsala University, Department of Engineering Sciences, 2019. [Online]. Available: https://www.diva-portal.org/smash/get/diva2:1313281/FULLTEXT01.pdf. [Accessed: 23-Jul-2025].

[35] Epiroc, *Pit Viper 351 Brochure*, Epiroc, [Online]. Available: https://www.epiroc.com/content/dam/epiroc/rotary-blasthole-drill-rigs/brochures/9863%200007%2001%20Pit%20Viper%20351%20Brochure%20English%20Web.pdf. [Accessed: 23-Jul-2025].

[36] IEEE Power & Energy Society, "IEEE Guide for Voltage Sag Indices," *IEEE Standard 1564-2014*, 2014. doi: 10.1109/IEEESTD.2014.6810559.

[37] M. H. J. Bollen, *Solving Power Quality Problems: Voltage Sags and Interruptions*, IEEE Press, Piscataway, NJ, 2000. ISBN: 0-7803-4713-7.

[38] Electric Power Research Institute (EPRI), "Technology Assessment and Application Guide for Utility Voltage Sag Performance," Technical Report No. 3002029060, Palo Alto, CA, 2025. Available: https://www.epri.com/research/products/000000003002029060

[39] A. El Maghraoui, Y. Ledmaoui, O. Laayati, and A. Chebak, "Power Quality Analysis of an Open-Pit Mine Electrical Network: Case Study Benguerir MinEx," in *2023 IEEE EUROCON—20th International Conference on Smart Technologies*, 2023, pp. 1–6. doi: 10.1109/EUROCON56442.2023.10199053.

[40] K. McLeod and R. Papp, "Common Power Quality Disturbances in Metals and Mining Facilities," *Electrical Products & Solutions*, 2023. Available: `https://epsmag.net/cover-story/common-power-quality-disturbances-in-metals-and-mining-facilities/` [Accessed: 24-Jul-2025].

[41] P. Kundur, *Power System Stability and Control*. New York, NY: McGraw-Hill, 1994.

[42] M. M. Ismail, B. M. Elhady, and A. Bendary, "Variable Voltage Control of Three-Phase Induction Motor for Energy Saving," *ERJ. Engineering Research Journal*, vol. 44, no. 4, pp. 377–383, 2021, Menoufia University, Faculty of Engineering.

[43] Microchip Technology Inc., "Sensorless Field Oriented Control (FOC) of an AC Induction Motor (ACIM)," Application Note AN1162, March 2010. [Online]. Available: `https://tungvp.wordpress.com/wp-content/uploads/2010/03/an1162-sensorless-field-oriented-control-foc-of-an-ac-induction-motor-acim.pdf`

[44] Devanshu, A., Singh, M., and Kumar, N., "An Improved Nonlinear Flux Observer Based Sensorless FOC IM Drive With Adaptive Predictive Current Control," *IEEE Transactions on Power Electronics*, vol. 35, no. 1, pp. 652–666, 2020. doi: 10.1109/TPEL.2019.2912265.

[45] Kubota, H. and Matsuse, K., "Speed sensorless field oriented control of induction machines using flux observer," in *Proceedings of IECON'94 - 20th Annual Conference of IEEE Industrial Electronics*, vol. 3, pp. 1611–1615, 1994. doi: 10.1109/IECON.1994.398054.

[46] S. Z. Djokic, K. Stockman, J. V. Milanovic, J. J. M. Desmet, and R. Belmans, "Sensitivity of AC adjustable speed drives to voltage sags and short interruptions," *IEEE Transactions on Power Delivery*, vol. 20, no. 1, pp. 494–505, Jan. 2005, doi: 10.1109/TPWRD.2004.832353.

[47] D. A. Paice, "Calculation of Harmonics," in *Power Electronics Converter Harmonics: Multipulse Methods for Clean Power*, 1996, pp. 97–121, doi: 10.1109/9780470545560.ch7.

[48] N. I. Nahin, M. Nafis, S. P. Biswas, M. K. Hosain, P. Das, and S. Haq, "Investigating the input power quality of multi-pulse AC–DC power converter fed induction motor drives," *Heliyon*, vol. 8, no. 12, p. e11733, 2022, doi: 10.1016/j.heliyon.2022.e11733.

[49] ABB, "Active front end drive versus passive filter – Comparison of harmonic mitigation technology," Tech. Note 073, Rev. A, Effective Sept. 30 2021, 5 pp. [Online]. Available: `https://library.e.abb.com/public/5eb87f704cc14fa596fb610f5dfb27a3/LVD-EOTKN073U-EN_REVA.pdf`

[50] International Electrotechnical Commission, *IEC 60038:2009+AMD1:2021 CSV – IEC standard voltages*, Edition 7.1, IEC, Geneva, Switzerland, Dec. 2021,ISBN: 9782832240281, doi: 10.3403/IEC60038.2009+AMD1.2021.

[51] International Electrotechnical Commission, "IEC 61000-4-30: Electromagnetic compatibility (EMC) – Part 4-30: Power quality measurement methods," IEC, Geneva, Switzerland, Edition 3.0, 2015, doi: 10.3403/IEC61000-4-30.2015.

DEPARTMENT OF SOME SUBJECT OR TECHNOLOGY
CHALMERS UNIVERSITY OF TECHNOLOGY
Gothenburg, Sweden
www.chalmers.se

CHALMERS
UNIVERSITY OF TECHNOLOGY